Cell Metabolism

Article

Gut microbial co-metabolite 2-methylbutyrylcarnitine exacerbates thrombosis via binding to and activating integrin α2β1

Graphical abstract

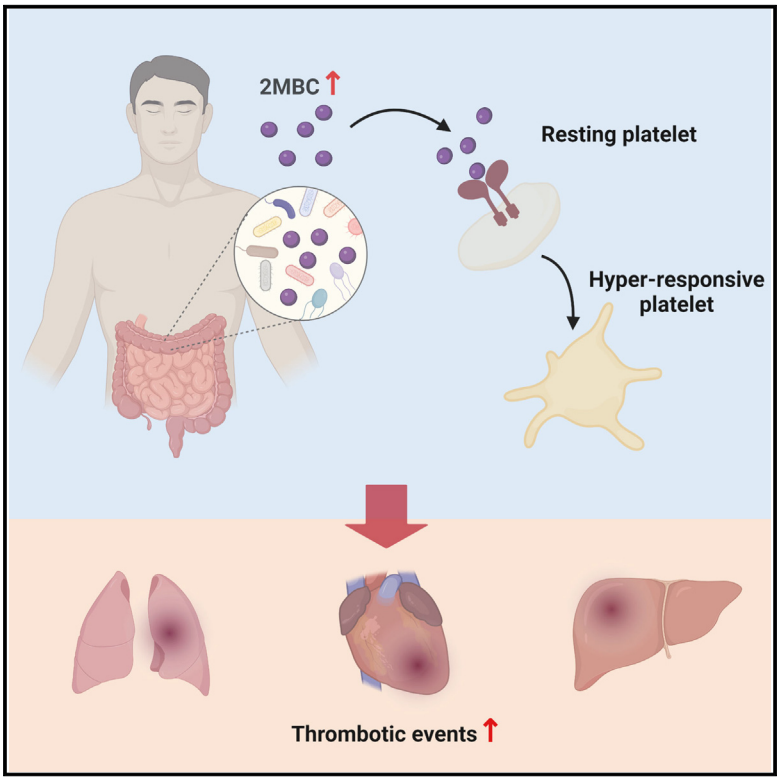

Highlights

- 2MBC accumulation leads to increased thrombotic risk
- 2MBC directly binds to integrin α2β1 and potentiates platelet hyperreactivity
- Inhibition of integrin α2β1 ameliorates 2MBC-induced heightened thrombotic risk
- 2MBC is a co-metabolite bridging gut microbiota dysbiosis and thrombosis

Authors

Kan Huang, Zilun Li, Xi He, ..., Meng Ren, Linghua Li, Sifan Chen

Correspondence

renmeng80@139.com (M.R.), llheliza@126.com (L.L.), chensf26@mail.sysu.edu.cn (S.C.)

In brief

Huang et al. demonstrate that 2MBC, a host and gut microbial co-metabolite, is positively associated with thrombotic risk in humans. Their study elucidates that 2MBC potentiates platelet hyperreactivity through integrin α2β1 and indicates that 2MBC is a metabolite that potentially links gut microbiota dysbiosis to an increased risk of thrombosis.

Huang et al., 2024, Cell Metabolism *36*, 1–19
March 5, 2024
https://doi.org/10.1016/j.cmet.2024.01.014

CellPress

Please cite this article in press as: Huang et al., Gut microbial co-metabolite 2-methylbutyrylcarnitine exacerbates thrombosis via binding to and activating integrin α2β1, Cell Metabolism (2024), https://doi.org/10.1016/j.cmet.2024.01.014

Cell Metabolism

CellPress

Article

Gut microbial co-metabolite 2-methylbutyrylcarnitine exacerbates thrombosis via binding to and activating integrin α2β1

Kan Huang,[1,2,3,4,19] Zilun Li,[3,4,19] Xi He,[5,19] Jun Dai,[6,19] Bingding Huang,[7,19] Yongxia Shi,[6,19] Dongxiao Fan,[3,4] Zefeng Zhang,[1,2] Yunchong Liu,[3,4] Na Li,[3,4] Zhongyu Zhang,[1,2] Jiangyun Peng,[1,2] Chenshu Liu,[3,4] Renli Zeng,[1,2] Zhipeng Cen,[1,2] Tengyao Wang,[1,2] Wenchao Yang,[3,4] Meifeng Cen,[1] Jingyu Li,[7] Shuai Yuan,[6] Lu Zhang,[6] Dandan Hu,[6] Shuxiang Huang,[6] Pin Chen,[8] Peilong Lai,[9] Liyan Lin,[1,2] Jielu Wen,[1,2] Zhengde Zhao,[3,4] Xiuyi Huang,[3,4] Lining Yuan,[1,2] Lifang Zhou,[1,2] Haoliang Wu,[3,4] Lihua Huang,[1,2] Kai Feng,[5] Jian Wang,[5] Baolin Liao,[5] Weiping Cai,[5] Xilong Deng,[5] Yueping Li,[5] Jianping Li,[5] Zhongwei Hu,[5] Li Yang,[5] Jiaojiao Li,[5] Youguang Zhuo,[5] Fuchun Zhang,[5] Lin Lin,[10] Yifeng Luo,[11] Wei Zhang,[12] Qianlin Ni,[12] Xiqiang Hong,[12] Guangqi Chang,[3,4] Yang Zhang,[13] Dongxian Guan,[14] Weikang Cai,[15] Yutong Lu,[8] Fang Li,[16] Li Yan,[17,18] Meng Ren,[17,18,*] Linghua Li,[5,*] and Sifan Chen[1,2,20,*]

[1]Guangdong Provincial Key Laboratory of Malignant Tumor Epigenetics and Gene Regulation, Guangdong-Hong Kong Joint Laboratory for RNA Medicine, Medical Research Center, Sun Yat-Sen Memorial Hospital, Sun Yat-Sen University, Guangzhou, Guangdong 510120, China
[2]Nanhai Translational Innovation Center of Precision Immunology, Sun Yat-Sen Memorial Hospital, Foshan, Guangdong 528200, China
[3]Division of Vascular Surgery, The First Affiliated Hospital of Sun Yat-Sen University, Guangzhou, Guangdong 510080, China
[4]National-Guangdong Joint Engineering Laboratory for Diagnosis and Treatment of Vascular Diseases, The First Affiliated Hospital of Sun Yat-Sen University, Guangzhou, Guangdong 510080, China
[5]Guangzhou Eighth People's Hospital, Guangzhou Medical University, Guangzhou, Guangdong 510060, China
[6]Guangzhou Customs District Technology Center, Guangzhou, Guangdong 510700, China
[7]College of Big Data and Internet, Shenzhen Technology University, Shenzhen, Guangdong 518118, China
[8]National Supercomputer Center in Guangzhou, School of Computer Science and Engineering, Sun Yat-Sen University, Guangzhou, Guangdong 510006, China
[9]Department of Hematology, Guangdong Provincial People's Hospital (Guangdong Academy of Medical Sciences), Southern Medical University, Guangzhou, Guangdong 510080, China
[10]Department of Respiratory Diseases, Sun Yat-Sen Memorial Hospital, Sun Yat-Sen University, Guangzhou, Guangdong 510120, China
[11]Department of Pulmonary and Critical Care Medicine, the First Affiliated Hospital of Sun Yat-sen University, Institute of Pulmonary Diseases, Sun Yat-sen University, Guangzhou, Guangdong 510080, China
[12]Wuhan Metware Biotechnology Co., Ltd., Wuhan, Hubei 430070, China
[13]School of Public Health, Sun Yat-Sen University, Shenzhen, Guangdong 518107, China
[14]Division of Endocrinology, Boston Children's Hospital, Harvard Medical School, Boston, MA 02115, USA
[15]Department of Biomedical Sciences, New York Institute of Technology, College of Osteopathic Medicine, Old Westbury, NY 11568, USA
[16]Department of Obstetrics and Gynecology, Guangzhou Women and Children Medical Center, Guangzhou Medical University, Guangzhou, Guangdong 510620, China
[17]Guangdong Clinical Research Center for Metabolic Diseases (Diabetes), Sun Yat-Sen Memorial Hospital, Sun Yat-Sen University, Guangzhou, Guangdong 510120, China
[18]Department of Endocrinology, Sun Yat-Sen Memorial Hospital, Sun Yat-Sen University, Guangzhou, Guangdong 510120, China
[19]These authors contributed equally
[20]Lead contact
*Correspondence: renmeng80@139.com (M.R.), llheliza@126.com (L.L.), chensf26@mail.sysu.edu.cn (S.C.)
https://doi.org/10.1016/j.cmet.2024.01.014

SUMMARY

Thrombosis represents the leading cause of death and disability upon major adverse cardiovascular events (MACEs). Numerous pathological conditions such as COVID-19 and metabolic disorders can lead to a heightened thrombotic risk; however, the underlying mechanisms remain poorly understood. Our study illustrates that 2-methylbutyrylcarnitine (2MBC), a branched-chain acylcarnitine, is accumulated in patients with COVID-19 and in patients with MACEs. 2MBC enhances platelet hyperreactivity and thrombus formation in mice. Mechanistically, 2MBC binds to integrin α2β1 in platelets, potentiating cytosolic phospholipase A2 (cPLA2) activation and platelet hyperresponsiveness. Genetic depletion or pharmacological inhibition of integrin α2β1 largely reverses the pro-thrombotic effects of 2MBC. Notably, 2MBC can be generated in a gut-microbiota-dependent manner, whereas the accumulation of plasma 2MBC and its thrombosis-aggravating effect are largely ameliorated following antibiotic-induced microbial depletion. Our study implicates 2MBC as a metabolite that links gut microbiota dysbiosis to elevated thrombotic risk, providing mechanistic insight and a potential therapeutic strategy for thrombosis.

Please cite this article in press as: Huang et al., Gut microbial co-metabolite 2-methylbutyrylcarnitine exacerbates thrombosis via binding to and activating integrin α2β1, Cell Metabolism (2024), https://doi.org/10.1016/j.cmet.2024.01.014

INTRODUCTION

Thrombosis represents the leading cause of death and disability upon major adverse cardiovascular events (MACEs), i.e., myocardial infarction, ischemic stroke, and pulmonary embolism. Platelet hyperreactivity is one of the most crucial factors contributing to thrombus formation and disseminated ischemia.[1,2] Accumulating evidence has documented hyperreactive functional response in platelets in the setting of numerous conditions, such as diabetes, obesity, hyperlipidemia, hypertension, or virus infection.[1,3–6] For instance, the outbreak of COVID-19 has led to a sharp increase in thrombotic events.[7] Notably, the hyperreactivity of platelet and its associated heightened thrombotic burden were not only present during acute phase but also remained in patients even after virus clearance,[8–11] highlighting that undisclosed nonclassical pathways, which are distinct from viral attack or acute inflammatory reaction, might be involved in the regulation of platelet activity. Hence, studies in patients with COVID-19 would be helpful in pinpointing new mechanisms contributing to thrombosis.

Extensive evidence has shown an association between gut microbiota dysbiosis and heightened thrombosis potential.[12,13] As previously reported, gut microbiota-derived metabolites, i.e., trimethylamine-N-oxide (TMAO) and phenylacetyl glutamine (PAGln), can increase platelet activity and thrombus formation, as well as the risk of cardiovascular diseases.[12,14–17] Despite the fact that gut microbiota dysbiosis has been intensively described in patients with COVID-19[18–20] and metabolic disorders[21–23] associated with heightened thrombotic risk, their causal link and the mechanisms contributing to thrombotic complications remain poorly understood.

Herein, we conducted multi-metabolomic analyses and identified 2-methylbutyrylcarnitine (2MBC), a short branched-chain acylcarnitine, as a critical host and gut microbial co-metabolite contributing to the heightened thrombotic risk. 2MBC was shown to promote platelet hyperreactivity via directly binding to integrin α2β1, whereas genetic depletion or pharmacological inhibition of integrin α2β1 was sufficient to ameliorate the heightened thrombosis potential induced by 2MBC. Collectively, this study provides mechanistic insight and a potential treatment strategy for enhanced thrombotic risks.

RESULTS

Acylcarnitines (2MBC, IBC, and HXC) are associated with a high thrombotic risk in patients with COVID-19

Given that the alteration of gut microbiota may contribute to the acute and long-term complications of COVID-19,[19,24] we hypothesized that gut microbiota may impact thrombotic risk upon severe acute respiratory syndrome coronavirus 2 (SARS-CoV-2) infection. To test this, humanized ACE2 (hACE2)-transgenic mice (with replacement of endogenous mouse ACE2) were pre-treated with antibiotic cocktail in drinking water to deplete the intestinal microbiota and then inoculated intranasally with SARS-CoV-2. Intriguingly, viral infection robustly induced vascular thrombosis in lung, heart, and liver of hACE2 mice, whereas this tendency was largely ameliorated following antibiotic-induced microbial depletion (Figure S1A), indicating a potential causal link between gut microbiota and the heightened thrombotic risk in COVID-19. As is well documented, gut microbiota influences host physiology mainly through the production of various metabolites.[25] We therefore speculated that gut microbiota-derived metabolites may play a role in mediating the heightened thrombotic potential in patients with COVID-19. To investigate the alteration of gut metabolites in patients with COVID-19, fecal samples from two different cohorts were collected for untargeted metabolomics analysis (Figure 1A). Cohort 1 was designed to identify the altered metabolites during the acute phase of SARS-CoV-2 infection. Individuals with COVID-19 (n = 64, 30 non-severe and 34 severe cases), healthy (n = 12), or non-COVID-19 hospitalized during the same period (n = 12) were enrolled (see Tables S1 and S2 for clinical data). Orthogonal partial least-squares discriminant analysis (OPLSDA) showed robust alterations of fecal metabolite composition in patients with COVID-19 in comparison with healthy or non-COVID-19 groups (Figure S1B). Among the 772 metabolites identified, 79 metabolites were upregulated while 121 were downregulated in COVID-19 in comparison with healthy individuals, while a significant alteration was observed in COVID-19 in comparison with non-COVID-19 subjects as well (fold change > 1.5 and VIP > 1; Figures S1C and S1D). Cohort 2 was designed to investigate the dynamic alterations of fecal metabolites at different periods of COVID-19. Fecal samples from patients with COVID-19 (n = 28, 12 non-severe and 16 severe cases) during the acute phase, quarantine, and convalescence were consecutively collected, whereas fecal samples from healthy individuals were used as controls (n = 12). OPLSDA showed that fecal metabolites were altered not only at acute phase but also at quarantine and convalescence when the virus was completely cleared (Figures S2E–S2G). The changes of fecal metabolites at different stages were shown in volcano plots (Figures S1H–S1J). Taken together, these data demonstrate a persistent alteration of fecal metabolites in patients with COVID-19.

We then speculated that the altered metabolites may be involved in the regulation of COVID-19 complications. Unexpectedly, our observation (data not shown) along with a study of serum metabolomic analysis[26] indicated that the well-recognized pro-thrombotic gut microbiota-dependent metabolites (TMAO and PAGln) were not altered in patients with COVID-19, implying that there might be other unidentified metabolites mediating this process. We then hypothesized the "culprit" metabolites contributing to the long-term adverse effects in COVID-19 should meet the following criteria: (1) significantly elevated in both non-severe and severe groups in comparison with healthy and non-COVID-19 groups (64 metabolites identified) and (2) sustainably upregulated throughout the acute, quarantine, and convalescent stages in the non-severe group (62 metabolites) or in the severe group (41 metabolites) (Figures 1B–1D). Among these, 9 metabolites met all the above-mentioned criteria (Figure 1E). Their relative abundances in each cohort are illustrated in Figures 1F, 1G, and S2A–S2C (also see Table S3 for mass spectrometry information). Logistic regression analysis was applied to adjust the potential bias factors. After adjusting for age, gender, BMI, hypertension, hyperlipidemia, and diabetes, all the metabolites still showed significant differences in non-severe and severe groups compared with the healthy control group ($p < 0.05$), except for uridine 5-monophosphate ($p = 0.1699$) and

Please cite this article in press as: Huang et al., Gut microbial co-metabolite 2-methylbutyrylcarnitine exacerbates thrombosis via binding to and activating integrin α2β1, Cell Metabolism (2024), https://doi.org/10.1016/j.cmet.2024.01.014

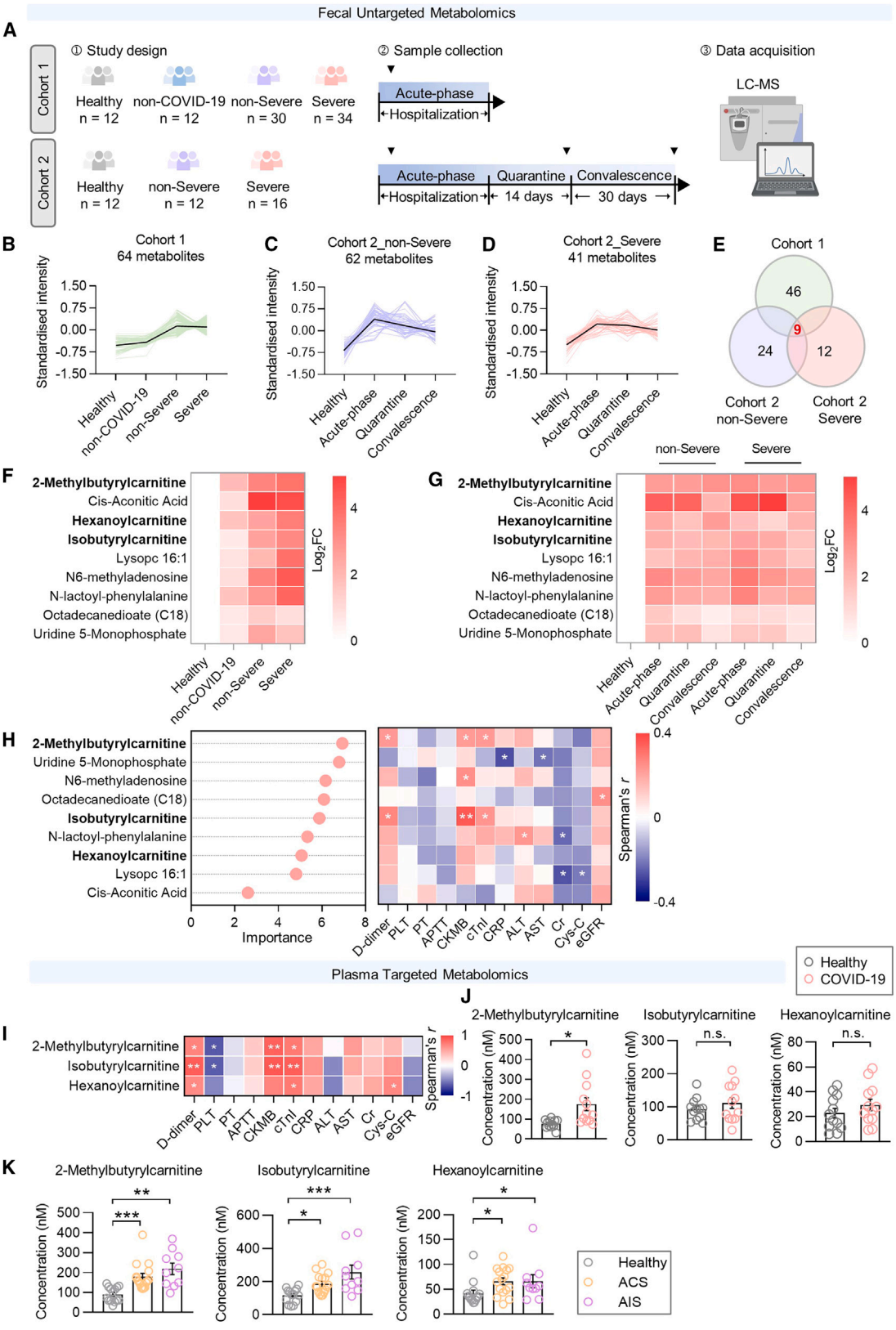

(legend on next page)

Please cite this article in press as: Huang et al., Gut microbial co-metabolite 2-methylbutyrylcarnitine exacerbates thrombosis via binding to and activating integrin α2β1, Cell Metabolism (2024), https://doi.org/10.1016/j.cmet.2024.01.014

Lysopc 16:1 (p = 0.0835), between the severe and healthy groups (Figure S2D). Notably, among the 9 metabolites, 2MBC (C5 acylcarnitine), isobutyrylcarnitine (IBC, C4 acylcarnitine), and hexanoylcarnitine (HXC, C6 acylcarnitine) belong to the acylcarnitine family, a subset of esters that transport acyl groups into the mitochondrial matrix for energy production. In particular, 2MBC was ranked as the most important classifier variable among these 9 metabolites in separating patients with COVID-19 from healthy or non-COVID-19 individuals as indicated by random forest algorithm (Figure 1H). Importantly, 2MBC and IBC were positively correlated with clinical parameters associated with thrombotic cardiovascular diseases (D-dimer, creatine kinase-MB [CKMB], and cardiac troponin I [cTnI]) ($p < 0.05$), whereas HXC showed a similar, yet non-significant, correlation ($p > 0.05$) (Figure 1H). Taken together, our data suggest a strong link between these three acylcarnitines and the increased thrombotic risk in COVID-19.

Given that plasma 2MBC, IBC, and HXC are elevated in multiple metabolic diseases, including obesity,[27] diabetes,[27,28] and hypertension,[29] we next measured their levels in patients with COVID-19 at acute phase and conducted a correlation analysis with corresponding clinical parameters. Despite positive correlations between plasma levels of these three metabolites and D-dimer, CKMB, and cTnI (Figure 1I), only plasma levels of 2MBC were significantly elevated (2.2-fold, p = 0.0120) in patients with COVID-19 compared with the healthy controls (Figure 1J). In addition, IBC (1.2-fold, p = 0.3420) and HXC (1.3-fold, p = 0.2869) showed a similar trend toward elevation in plasma (Figure 1J). Moreover, plasma 2MBC was elevated in patients with non-COVID-19 severe pneumonia (Figure S2E), indicating that the elevation of 2MBC is not specific to SARS-CoV-2 infection. To further investigate whether the aberrant accumulation of 2MBC, IBC, and HXC is associated with thrombotic potential in patients without SARS-CoV-2 infection, an independent cohort of MACEs was enrolled. Plasma levels of these three acylcarnitines were significantly elevated in patients with acute coronary syndrome (ACS) and acute ischemic stroke (AIS) (Figure 1K), suggesting that these species may play an important role in triggering thrombotic events in patients with cardiovascular diseases as well. Finally, we confirmed that intraperitoneal (i.p.) injection of 2MBC, IBC, or HXC accelerated thrombus generation in $FeCl_3$-induced carotid artery thrombosis in mice (Figure S2F). Taken together, our data illustrate that short-branched or medium-chain acylcarnitines, especially 2MBC, might represent crucial metabolites leading to an increased thrombotic risk.

2MBC enhances thrombotic potential *in vivo*

To determine the impact of 2MBC on thrombus formation *in vivo*, multiple mouse models of thrombosis were employed. First, $FeCl_3$ induced carotid artery occlusion by 13 min on average in control animals. Pre-treatment of 2MBC either via i.p. injection (Figure 2A) or oral gavage (Figure S3A), however, was capable of shortening the occlusion time in a dose-dependent manner following $FeCl_3$-induced injury. Notably, a high dose of 2MBC injection (i.p., 100 μg/kg) reduced the time to cessation of flow within the carotid artery by nearly 50% (Figure 2A). Scattered plot of individual animals showed that the cessation times were negatively correlated with 2MBC levels in plasma (p = 0.0049; Figures S3B and S3C). Second, a photochemical carotid artery injury model also confirmed that the occlusion time declined by 38.6% following 2MBC administration (Figure 2B). Considering the high fatality of pulmonary embolism,[30] we explored the effect of 2MBC on thrombin-induced pulmonary artery thrombosis, established in a murine model that mimicked the fatal outcome of pulmonary embolism.[31] Intravenous injection of a sublethal dose of thrombin (200 U/kg) led to a mortality rate of 33.3% within 30 min, while pre-treatment of 2MBC significantly increased the mortality rate to 83.3% (Figure 2C). Moreover, the infarct size of lungs, indicated by staining of Evans blue dye, was significantly increased in 2MBC-treated mice (Figure S3D). The amounts of thrombi in lung tissues almost doubled in the 2MBC group in comparison with the control group (Figure 2D). In a complementary set of studies in which mice were subjected to a lower non-lethal dose of thrombin (40 U/kg), echocardiography showed that 2MBC administration elevated the mean pulmonary artery pressure and peak pulmonary velocity and shortened the peak attainment time in pulmonary arteries (Figures S3E and S3F). Plasma thromboxane B2 (TXB2), a thrombotic biomarker, was also significantly increased in 2MBC-treated mice (Figure S3G). These data imply that 2MBC exacerbates pulmonary artery thrombosis. We next sought to investigate the influence of 2MBC on venous thrombosis. Using the St. Thomas stenosis model,[32] we observed that plasma D-dimer was significantly elevated in the 2MBC group (Figure S3H), despite the lack of changes in the incidence of inferior vena cava thrombosis and the weight of thrombi (data not shown). Finally, tail bleeding assay revealed a significant reduction of blood loss in 2MBC-treated mice (Figure S3I). Taken together, our *in vivo* data from multiple mouse models of thrombosis strongly indicate that 2MBC robustly enhances the risk of thrombosis.

The activation of platelet and coagulation cascade is the main cause of thrombosis. To further explore the underlying

Figure 1. Acylcarnitines (2MBC, IBC, and HXC) are associated with high thrombotic risk in patients with COVID-19

(A) Study design and workflow summary. Upper black triangles indicate sample collection time of each group.

(B–E) Metabolites screening from cohort 1 (B) and cohort 2 (C and D) related to healthy or non-COVID-19 group. Black line indicates mean standard intensity of the metabolites of each cluster. Venn diagram indicates 9 shared metabolites overlapped in these 3 clusters (E).

(F and G) The relative abundances of the 9 metabolites (shown in alphabetical order) in different groups of cohort 1 (F) and cohort 2 (G). Log_2 fold change (FC) was calculated against the healthy group.

(H) Random forest analysis of the 9 metabolites (left) and Spearman correlation analysis between metabolite abundances and plasma biochemistry parameters of patients with COVID-19 in cohort 1 (right).

(I) Correlations between plasma levels of the 3 acylcarnitine species and plasma biochemistry parameters in patients with COVID-19 (n = 12).

(J) Plasma levels of 2MBC, IBC, and HXC between healthy individuals and patients with COVID-19 (n = 12).

(K) Plasma levels of 2MBC, IBC, and HXC among healthy individuals (n = 14), ACS (n = 16), and AIS patients (n = 10).

Data points represent the means ± SEM. Statistics used unpaired Student's t test (J) or one-way ANOVA with Fisher's LSD post hoc test (K). n.s., not significant; *p < 0.05; **p < 0.01; ***p < 0.001.

Please cite this article in press as: Huang et al., Gut microbial co-metabolite 2-methylbutyrylcarnitine exacerbates thrombosis via binding to and activating integrin α2β1, Cell Metabolism (2024), https://doi.org/10.1016/j.cmet.2024.01.014

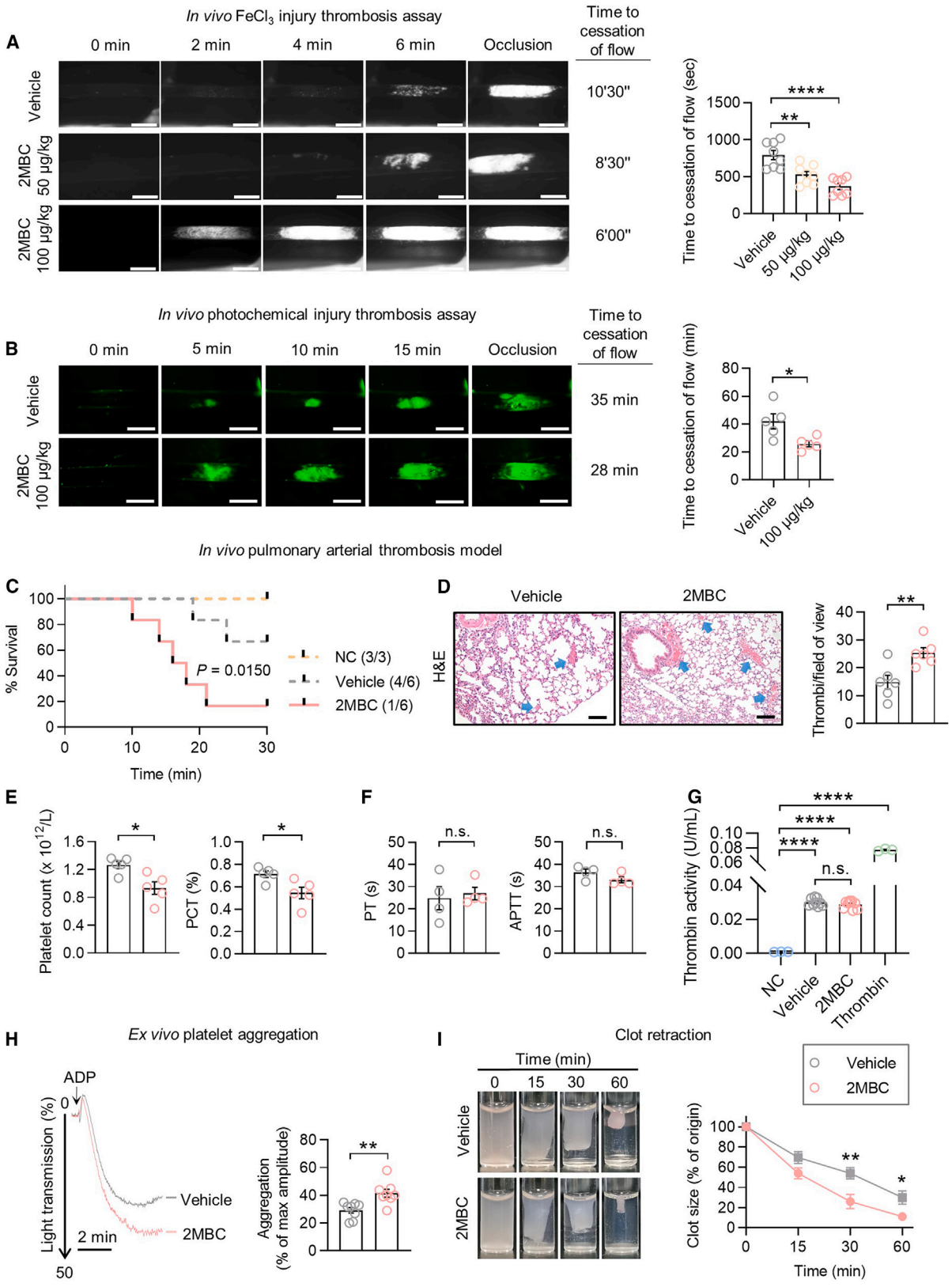

(legend on next page)

Please cite this article in press as: Huang et al., Gut microbial co-metabolite 2-methylbutyrylcarnitine exacerbates thrombosis via binding to and activating integrin α2β1, Cell Metabolism (2024), https://doi.org/10.1016/j.cmet.2024.01.014

mechanisms of the pro-thrombotic effect of 2MBC, blood count and coagulation indices were examined following i.p. injection of 2MBC. We found 2MBC administration significantly decreased the platelet count and plateletcrit in peripheral blood (Figure 2E) and modestly increased the platelet distribution width (Figure S3J), suggesting the hyperreactivity and subsequential consumption of platelets. In contrast, the prothrombin time, activated partial thromboplastin time (Figure 2F), and thrombin activity (Figure 2G) were not altered. These data suggest that 2MBC may exert pro-thrombotic effect via modulating platelet function, rather than coagulation function, in mice. To test this, platelet-rich plasma (PRP) isolated from mice pre-treated with 2MBC or vehicle was subjected to *ex vivo* platelet aggregometry and clot retraction assay. In response to adenosine diphosphate (ADP) stimulation, 2MBC increased platelet aggregation by 42% (Figure 2H) and significantly enhanced clot contraction (Figure 2I). In addition, treatment with the anti-platelet reagent aspirin prominently ameliorated the aggravating effect of 2MBC on thrombogenesis, as indicated by *in vivo* $FeCl_3$ injury thrombosis assay (Figure S3K) and pulmonary artery thrombosis assay (Figures S3L and S3M), whereas the anti-coagulant heparin displayed a limited effect (Figures S3K–S3M). Furthermore, 6-week administration of 2MBC did not affect plasma inflammatory cytokines such as ferritin and interleukin-6 in mice (Figure S3N), which were thought to be associated with thrombosis.[33,34] Collectively, our results suggest that 2MBC may promote thrombotic potential via enhancing platelet reactivity.

2MBC promotes platelet hyperresponsiveness by enhancing cPLA2 activation

To clarify whether exogenous 2MBC could directly modulate platelet function, rat PRP was isolated for a series of *in vitro* assays. Platelet aggregometry showed that 2MBC potentiated platelet aggregation in a dose-dependent manner in response to a submaximal concentration of ADP (2 μM) stimulation (Figure 3A). Notably, the effect of 0.5 μM 2MBC on platelet aggregation was comparable to that of 100 μM TMAO, a potent metabolite to promote platelet hyperreactivity (Figure S4A). Moreover, following stimulation of various concentrations of ADP, 2MBC remarkably enhanced platelet aggregation (Figure 3B), which was further confirmed in human PRP (Figure 3C) or washed rat platelets (Figure S4B). A similar potentiating effect of 2MBC on platelet aggregation was also observed in washed platelets or PRP exposed to diverse agonists (thrombin, or ADP plus collagen) at various doses (Figures 3D–3F, S4C, and S4D). We then assessed platelet spreading on immobilized collagen. Pre-incubation of 2MBC significantly increased the adhesive interaction between platelet and collagen matrix by 94.5% (Figure 3G). Furthermore, the clot size was reduced by 40% at 60 min in the presence of 2MBC, indicating an enhancement of platelet clot retraction (Figure 3H). Collectively, these data indicate that 2MBC promotes platelet hyperresponsiveness.

Thromboxane A2 (TXA2), an unstable arachidonic acid (AA) metabolite, is well recognized for its ability to amplify initial platelet activation process.[35,36] As expected, pre-incubation of 2MBC significantly increased the level of TXB2, a stable derivative of TXA2, in response to ADP (Figure 3I). Importantly, the effect of 2MBC on platelet aggregation was largely inhibited by aspirin, a cyclooxygenase 1 inhibitor that suppresses the generation of TXA2[37] (Figure 3J). These data indicate an essential role of TXA2 in mediating the effect of 2MBC on platelet hyperresponsiveness. In platelet, cytosolic phospholipase A2 (cPLA2), which is regulated by mitogen-activated protein kinase (MAPK) signaling (i.e., ERK or p38),[10] is mainly responsible for AA liberation and subsequent production to TXA2[38,39] (Figure 3K). Our data showed that 2MBC significantly potentiated ADP- and thrombin-induced phosphorylation of cPLA2 and p38 MAPK, whereas no alteration on p-ERK was observed in a 2MBC-dependent manner (Figures 3L and S4E). Importantly, the enhancing effect of 2MBC on platelet aggregation was largely blocked by cPLA2 inhibitor methyl arachidonyl fluorophosphonate (MAFP) (Figures 3M and S4F). In line with that, the induction of AA liberation by 2MBC was completely reversed in the presence of MAFP (Figure 3N). Taken together, our data suggest that 2MBC promotes platelet hyperresponsiveness via enhancing cPLA2 activation.

2MBC directly binds to and potentiates integrin α2β1 activation

We further investigated the mechanism by which 2MBC potentiates cPLA2 activation and enhances platelet reactivity. Acylcarnitines are responsible for the transport of acyl groups from fatty acids across the inner mitochondrial membrane for β-oxidation,[40] which may promote the activation of platelets.[41] Therefore, we asked whether 2MBC supplementation influenced fatty acid oxidation (FAO) in platelets. The FAO was not altered in the presence of 2MBC at indicated concentrations in platelets, as well as in the HEK-293T and HeLa cells, whereas it was significantly enhanced upon oleate treatment (Figures S5A–S5C).

Figure 2. 2MBC enhances thrombotic potential *in vivo*

(A and B) Representative images of carotid artery thrombus formation at the indicated time points and quantification of time to flow cessation following $FeCl_3$-induced carotid artery injury (A, n = 8) or photochemical injury (B, n = 5) in mice i.p. injected with saline or indicated doses of 2MBC. Scale bars, 500 μm.

(C) Kaplan-Meier curves represent the survival rates of mice i.p. injected with saline or 2MBC (100 μg/kg) within 30 min following thrombin (200 U/kg) administration (n = 6). Mice injected with equal volume of saline instead of thrombin were set as negative control (NC, n = 3).

(D) Representative images of the lung sections and quantifications. Scale bars, 100 μm.

(E and F) Calculations of platelet count (left) and PCT (right) from peripheral blood (E, n = 5) and detections of PT (left) and APTT (right) in plasma (F, n = 4) after i.p. injection of saline or 100 μg/kg 2MBC.

(G) Detection of thrombin activity in plasma after i.p. injection of saline or 100 μg/kg 2MBC (n = 3 with 3 technical repeats); negative reagent was set as negative control and thrombin as positive control (n = 3).

(H and I) ADP (5 μM)-stimulated platelet aggregometry responses (H, n = 8) and clot retraction (I, n = 5) were monitored in mice PRP following i.p. pre-injected with saline or 100 μg/kg 2MBC.

Data points represent the means ± SEM. Statistics used Brown-Forsythe and Welch ANOVA followed by unpaired t test with Welch's correction (A and G), unpaired Student's t test (B, E, and H), log-rank (Mantel-Cox) test (C), Welch's t test (D and F), or two-way ANOVA with repeated measures (I). *$p < 0.05$; **$p < 0.01$; ****$p < 0.0001$.

Please cite this article in press as: Huang et al., Gut microbial co-metabolite 2-methylbutyrylcarnitine exacerbates thrombosis via binding to and activating integrin α2β1, Cell Metabolism (2024), https://doi.org/10.1016/j.cmet.2024.01.014

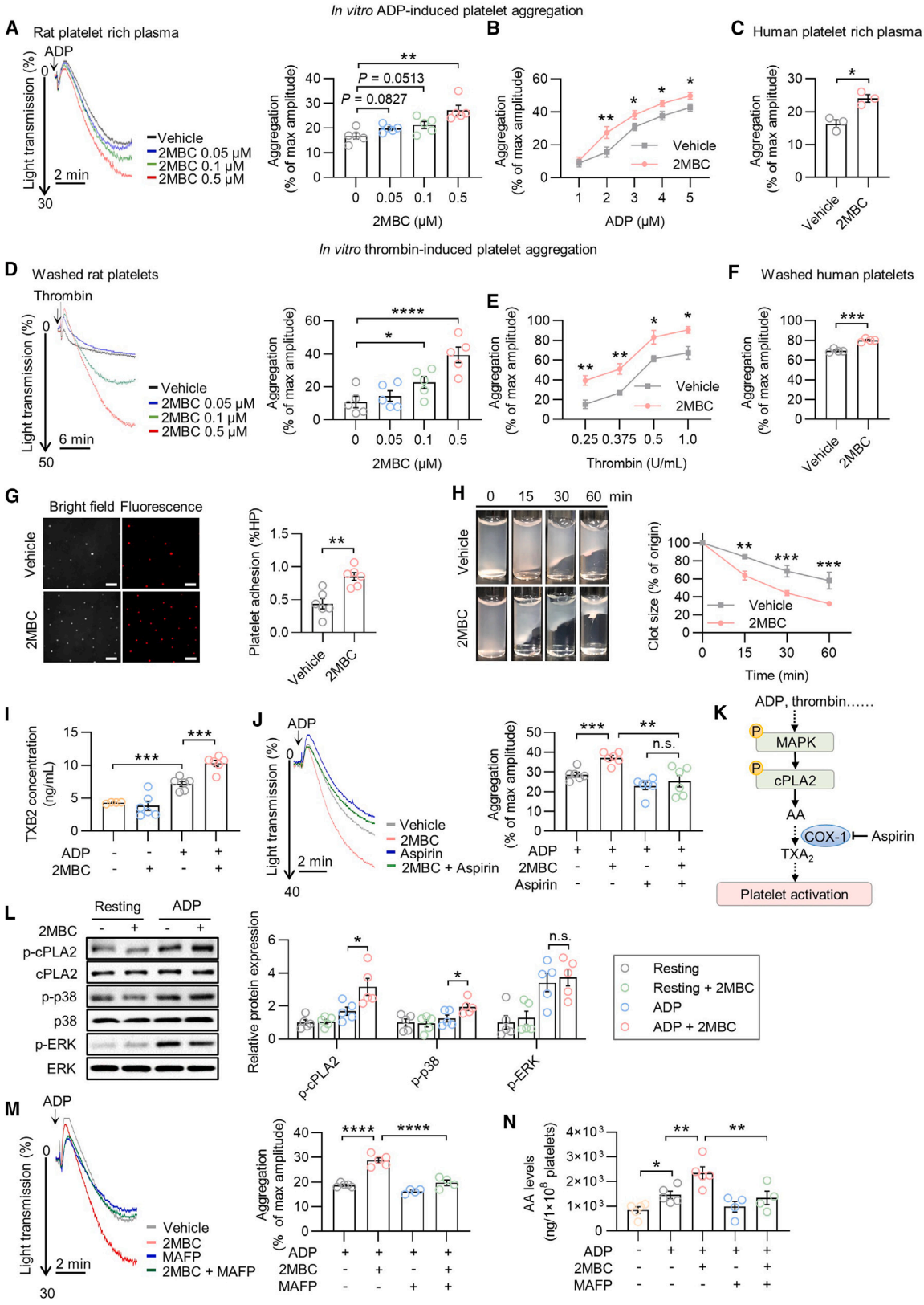

(legend on next page)

Please cite this article in press as: Huang et al., Gut microbial co-metabolite 2-methylbutyrylcarnitine exacerbates thrombosis via binding to and activating integrin α2β1, Cell Metabolism (2024), https://doi.org/10.1016/j.cmet.2024.01.014

These results suggest that the effect of 2MBC on platelet reactivity might be independent of FAO.

Given that protein phosphorylation plays an important role in the regulation of platelet activity, we next analyzed the phosphoproteomics in platelets treated with 2MBC to explore the molecular mechanisms. Treatment of 2MBC triggered dramatic alterations in total phosphoproteome in washed rat platelets under agonist stimulation (Figure S5D). Thus, the phosphorylation of 394 residues in 279 proteins was significantly upregulated, while that of 183 residues in 155 proteins was significantly downregulated in the 2MBC group (fold change > 1.5, VIP > 1; Figure 4A). String database[42] was applied to establish a protein-protein interaction network for the upregulated phosphorylated proteins (Figure S5E). The local network cluster results suggested the interactive proteins were mainly involved in the extracellular matrix (ECM)-receptor interaction and integrin-mediated signal, etc. (Figure S5F). KEGG enrichment analysis showed that differentially phosphorylated proteins were enriched in the platelet activation pathway (Figure S5G). Moreover, the top enriched Reactome pathways included the downstream signaling pathways mediated by platelet membrane receptors (integrins, P2Y1, and GPIb-IX-V) (Figure 4B). The signaling pathways mediated by integrins are involved in regulation of platelet activation, aggregation, and adhesion, among which collagen receptor integrin α2β1 and fibrinogen receptor integrin αIIbβ3 play the most important role.[43–45] In parallel, P2Y1 and GPIb-IX-V, the corresponding receptors of ADP and von Willebrand factor, also play important roles in promoting platelet activation.[46,47] Downstream of these four critical receptors (Figure 4C), the phosphorylation of many key kinases including PKCα, Src, Pyk2, and PLCβ, was significantly upregulated after 2MBC treatment (Figure 4D). Consistent with our previous results (Figures 3L and S4E), the phosphorylation of cPLA2 and its upstream p38 MAPK was also significantly upregulated in the 2MBC group (Figure 4D). These omics data, such as phosphorylation of Src and PLCβ, were further verified by immunoblotting (Figure S5H).

Given the strong regulations of signaling cascades downstream of membrane receptors such as integrin α2β1, integrin αIIbβ3, P2Y1, or GPIb-IX-V, we postulated that 2MBC may directly bind to and activate one or more of these receptors. To test this hypothesis, we first knocked down the genes encoding the main ligand-binding subunits of integrin α2β1 (*ITGA2*), integrin αIIbβ3 (*ITGA2B*), GPIb-IX-V (*GP1BA*), or P2Y1 (*P2RY1*), in HEK-293T cells (Figure S5I). We found that depletion of *ITGA2*, but not the other three, was sufficient to abrogate 2MBC-induced cPLA2 phosphorylation (Figure S5J). When administered pharmacological compounds to block these receptors, only BTT 3033 (integrin α2β1 inhibitor), but not tirofiban (integrin α2IIbβ3 inhibitor) or BPTU (P2Y1 inhibitor), completely eliminated the effect of 2MBC on promoting platelet aggregation (Figure 4E). GPIb-IX-V inhibitor was not used as it was not commercially available. Additionally, BTT 3033 abolished the accentuated effects of 2MBC on platelet adhesion (Figure 4F) and cPLA2 phosphorylation (Figure 4G). These results suggest that integrin α2β1 is the likely target mediating the effects of 2MBC on cPLA2 hyper-phosphorylation and platelet hyperresponsiveness.

To further clarify whether 2MBC directly binds to integrin α2β1, we first performed virtual docking simulation using VSTH, a structure-based virtual screening web server on Tianhe-2 supercomputer,[48] and showed that 2MBC might directly interact with integrin α2β1 I domain (PDB: 1AOX), a ligand-binding domain mediating integrin α2β1 activation. The *in silico* virtual docking simulation of the structural binding between 2MBC and I domain protein/amino acids is illustrated in Figure S5K. Surface plasmon resonance (SPR) assay showed that 2MBC could directly bind to purified recombinant integrin α2β1 (Figure S5L) with a dissociation constant K_D value of 10.6 μM (Figures 4H and S5M), which is similar to the known integrin α2β1 ligand BTT 3033 (K_D = 11.0 μM) (Figures 4I and S5N). The negative control AA, on the other hand, failed to bind with integrin α2β1 (Figure 4J). The 2MBC-integrin α2β1 interaction appeared specific, as 2MBC could not bind to the ligand-binding domain of integrin αIIbβ3 (Figure 4K). Functionally, 2MBC significantly enhanced the phosphorylation of the proximal signaling kinases downstream of integrin α2β1,[49] including Src (Figure S5H) and FAK (Figure S5O), indicating the activation of integrin α2β1 following 2MBC binding under the stimulation of agonist. Supporting this, Src inhibitor A419259 largely blocked the enhancing effect of 2MBC on platelet aggregation (Figure S5P). Collectively, our data strongly suggest that 2MBC could directly bind to integrin

Figure 3. 2MBC promotes platelet hyperresponsiveness by enhancing cPLA2 activation

(A) ADP (2 μM)-stimulated platelet aggregometry responses in rat PRP pre-treated with saline or different doses of 2MBC (n = 5).
(B) ADP (up to 5 μM)-stimulated platelet aggregometry responses in rat PRP pre-treated with saline or 0.5 μM 2MBC (n = 5).
(C) ADP (2 μM)-stimulated platelet aggregometry responses in human PRP pre-treated with saline or 0.5 μM 2MBC (n = 3).
(D) Thrombin (1 U/mL)-stimulated platelet aggregometry responses in washed rat platelets pre-treated with saline or different doses of 2MBC (n = 5).
(E) Thrombin (up to 1 U/mL)-stimulated platelet aggregometry responses in washed rat platelets pre-treated with saline or 0.5 μM 2MBC (n = 5).
(F) Thrombin (1 U/mL)-stimulated platelet aggregometry responses in washed human platelets pre-treated with saline or 0.5 μM 2MBC (n = 4).
(G and H) Platelet spreading assay (G, n = 6) and clot retraction assay (H, n = 6) for rat PRP pre-incubated with saline or 0.5 μM 2MBC.
(I) ADP-induced changes of TXB2 in rat PRP with or without 2MBC (0.5 μM) pre-incubation (left to right: n = 4, 6, 6, and 6).
(J) ADP (2 μM)-stimulated platelet aggregometry responses in rat PRP pre-incubated with saline or 0.5 μM 2MBC in the presence or absence of aspirin (300 μM) (n = 6).
(K) Scheme illustrating cPLA2 pathway involved in the stimuli-induced platelet activation process.
(L) Changes of ADP (2 μM)-stimulated phosphorylation of cPLA2, p38, and ERK in rat PRP pre-treated with or without 0.5 μM 2MBC (n = 5).
(M) ADP (2 μM)-stimulated platelet aggregometry responses in rat PRP pre-incubated with saline or 0.5 μM 2MBC in the presence or absence of cPLA2 inhibitor MAFP (5 μM) (left to right: n = 5, 5, 4, and 4).
(N) ADP-induced changes of AA in rat PRP with saline or 0.5 μM 2MBC in the presence or absence of MAFP (5 μM) (left to right: n = 5, 5, 5, 4, and 4).
Data points represent the means ± SEM. Statistics used Brown-Forsythe and Welch ANOVA followed by unpaired t test with Welch's correction (A, I, J, and L), one-way ANOVA with Fisher's LSD post hoc test (D, M, and N), two-way ANOVA with Fisher's LSD post hoc test (B and E), or unpaired Student's t test (C, F, and G). n.s., not significant; *p < 0.05; **p < 0.01; ***p < 0.001; ****p < 0.0001.

Please cite this article in press as: Huang et al., Gut microbial co-metabolite 2-methylbutyrylcarnitine exacerbates thrombosis via binding to and activating integrin α2β1, Cell Metabolism (2024), https://doi.org/10.1016/j.cmet.2024.01.014

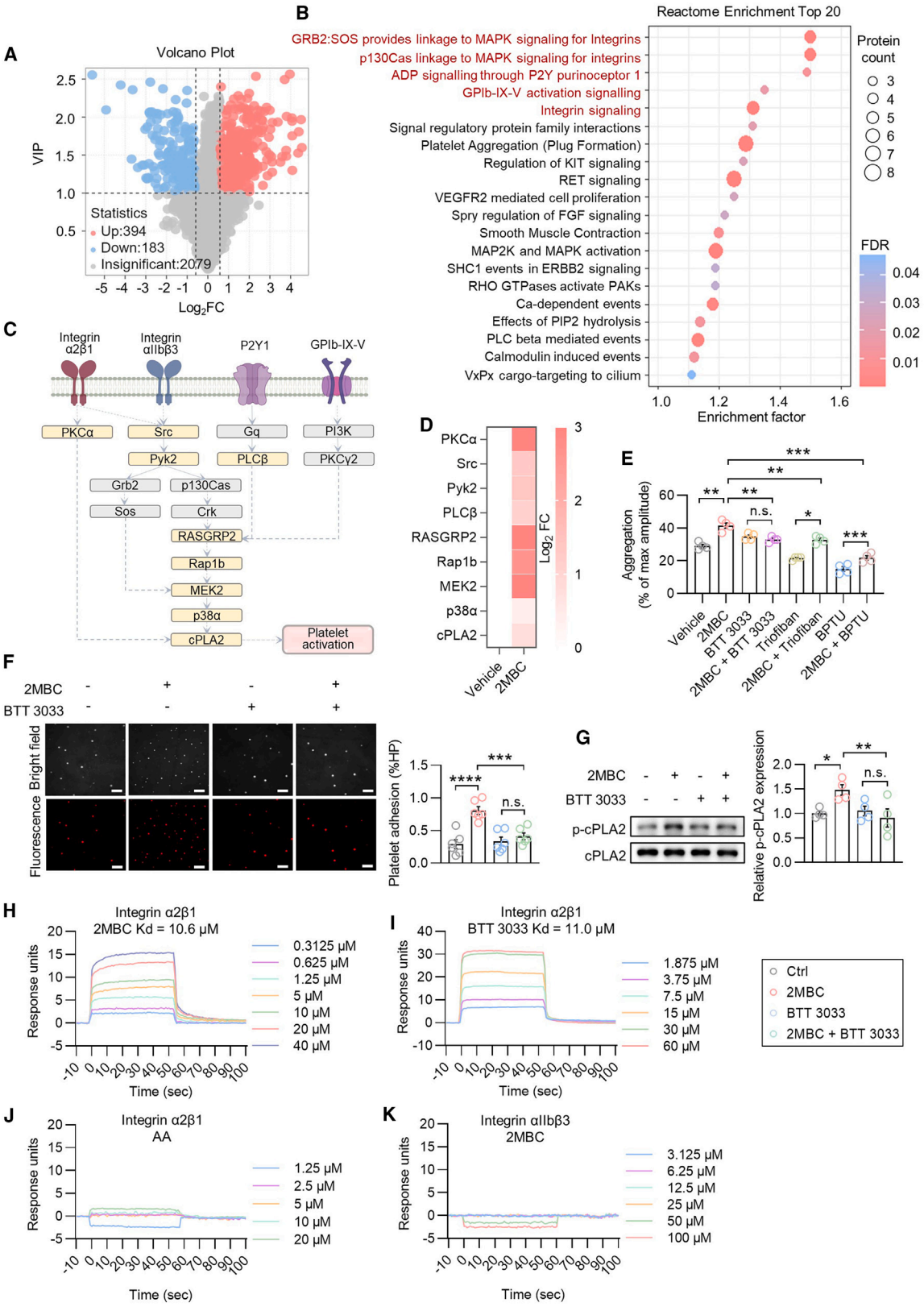

(legend on next page)

α2β1 and potentiate its downstream signal activation, thus regulating platelet responsiveness.

Genetic depletion or pharmacological inhibition of integrin α2β1 ameliorates the pro-thrombotic effect of 2MBC

To further determine whether integrin α2β1 is essential for the 2MBC-enhancing platelet reactivity, integrin α2 knockout (α2−/−) mice were established (Figure S6A). Importantly, we found that the thrombosis-accelerating effect of 2MBC was completely eliminated in α2−/− mice following $FeCl_3$ injury (Figure 5A). In line with the prior report,[50] loss of integrin α2 prolonged the cessation time of blood flow, albeit it was statistically insignificant (p = 0.1089) (Figure 5A). *In vitro* platelet aggregation (Figure 5B) and clot retraction assays (Figure 5C) revealed the enhanced platelet responses induced by 2MBC were substantially abrogated in the absence of integrin α2. Likewise, the 2MBC-mediated hyper-phosphorylated cPLA2 also vanished in α2−/− platelets (Figure S6B). These data confirm the integrin α2β1-dependent manner of 2MBC in provoking platelet hyperreactivity.

We then investigated the therapeutic potential for pharmacological inhibition of integrin α2β1. Using carotid artery injury thrombosis assay, we found that the thrombosis-accelerating effect of 2MBC was dose-dependently blocked by BTT 3033, a conformation-selective integrin α2β1 inhibitor that could not interact with other types of integrins[51] (Figures 5D and S6C). Consistently, immunohistochemical staining of thrombi within the carotid artery showed that 2MBC significantly increased the protein level of CD62P, a platelet activation marker, whereas this effect was almost completely blocked by BTT 3033 (Figures 5E and S6D). Likewise, BTT 3033 completely abrogated the 2MBC-induced phosphorylation of cPLA2 in the carotid thrombi (Figure S6E), as well as 2MBC-enhanced platelet aggregation responsiveness (Figure S6F). Furthermore, BTT 3033 remarkably increased the 30-min survival rate of mice from 33.3% to 87.5% in a pulmonary artery thrombosis mouse model pre-treated with 2MBC (Figure 5F), whereas the infarction area (Figure S6G) and the number of thrombi in lung tissues (Figure 5G) were robustly decreased. Notably, no toxic effects were observed upon BTT 3033 administration for 3 days, as determined by the measurement of plasma alanine aminotransferase, aspartate aminotransferase, and creatinine in mice (Figure S6H). Together, these results demonstrate that pharmacological inhibition of integrin α2β1 effectively ameliorates the thrombosis-enhancing effect of 2MBC *in vivo*.

We further explored the therapeutic potential of BTT 3033 in COVID-19. hACE2 mice fed with high-fat diet for 18 weeks were intranasally inoculated of SARS-CoV-2, followed by daily i.p. injections of BTT 3033 (1 mg/kg), and the body weight of mice after virus infection was illustrated in Figure S6I. Consistent with our previous finding (Figure S1A), thrombi were widely detectable in multiple organs including lung (Figures 5H and S6J), heart (Figures 5I and S6K), and liver (Figures 5J and S6L) after SARS-CoV-2 inoculation, as evidenced by H&E staining and CD62P reactivity. Notably, SARS-CoV-2-induced thrombosis in lung (Figures 5H and S6J), heart (Figures 5I and S6K), and liver (Figures 5J and S6L) was largely ameliorated by BTT 3033 treatment. Moreover, BTT 3033 partially protected lung from damage induced by SARS-CoV-2 infection (Figure 5K), but no alteration in viral load was observed (Figure S6M). The elevated thrombotic indices (i.e., D-dimer, TXB2, and soluble CD62P) and ischemic cardiac biomarker (cTnI) in plasma were all dramatically declined in the presence of BTT 3033 (Figure 5L). Together, these results consistently demonstrate that BTT 3033 ameliorates thrombosis induced by SARS-CoV-2 infection, indicating a potential therapeutic strategy for COVID-19-associated thrombotic events.

2MBC is an intermediate metabolite bridging gut microbiota dysbiosis and thrombotic events

We next sought to explore the potential origin of the elevated circulating 2MBC. 2MBC was previously characterized as an intermediate product of branched-chain amino acid (BCAA) catabolism in cells,[52–54] and catabolic defect of BCAA may lead to abnormal accumulation of 2MBC.[55,56] To determine whether BCAA catabolism is affected in injured tissues upon SARS-CoV-2 infection, RNA samples from heart, liver, and skeletal muscle from mice inoculated with SARS-CoV-2 were subjected to RT-qPCR analysis. Surprisingly, the expressions of key

Figure 4. 2MBC directly binds to and potentiates integrin α2β1 activation

(A) Phosphoproteomics analysis of washed rat platelets stimulated by thrombin (1 U/mL) after pre-incubated with saline or 0.5 μM 2MBC (n = 4). Volcano plots showed the differential phosphorylated residues between vehicle and 2MBC group (FC > 1.5, VIP > 1).

(B) Reactome enrichment analysis of phosphorylated proteins upregulated in 2MBC group and the top 20 pathways ranking by enrichment factor were shown. Red font in row title indicates the top 5 enrichment pathways.

(C) Scheme illustrating pathways mediated by membrane receptors integrin α2β1, integrin αIIbβ3, P2Y1, and GPIb-IX-V that were involved in the platelet activation process. Yellow frame represents the downstream phosphorylated proteins that have been detected in the current phosphoproteomics; gray frame represents the undetected downstream proteins. Solid arrow represents direct regulation of the proteins; dotted arrow represents indirect regulation of the proteins.

(D) Relative abundances of the phosphorylated proteins involved in integrin α2β1-, integrin αIIbβ3-, P2Y1-, and GPIb-IX-V-mediated pathway. Log_2 FC was calculated against vehicle group.

(E) ADP (2 μM)-stimulated platelet aggregometry responses in rat PRP pre-incubated with saline or 0.5 μM 2MBC in the presence or absence of BTT 3033 (1 μM, integrin α2β1 inhibitor), tirofiban (1 μM, integrin αIIbβ3 inhibitor), and BPTU (0.3 μM, P2Y1 inhibitor) (n = 4).

(F and G) Platelet spreading assay (F, n = 6) and western blotting analysis of cPLA2 phosphorylation (G, n = 4) for rat PRP pre-treated with saline or 0.5 μM 2MBC in the presence or absence of BTT 3033 (1 μM).

(H–K) Surface plasmon resonance (SPR) assay of purified integrin α2β1 protein with 2MBC (H), BTT 3033 (I, positive control), and arachidonic acid (J, negative control), or purified α2IIb ligand-binding domain protein with 2MBC (K).

Data points represent the means ± SEM. Statistics used Brown-Forsythe and Welch ANOVA followed by unpaired t with Welch's correction (E) or one-way ANOVA with Fisher's LSD post hoc test (F and G). n.s., not significant; *p < 0.05; **p < 0.01; ***p < 0.001; ****p < 0.0001. The schematic diagram in (C) was created by BioRender.

Please cite this article in press as: Huang et al., Gut microbial co-metabolite 2-methylbutyrylcarnitine exacerbates thrombosis via binding to and activating integrin α2β1, Cell Metabolism (2024), https://doi.org/10.1016/j.cmet.2024.01.014

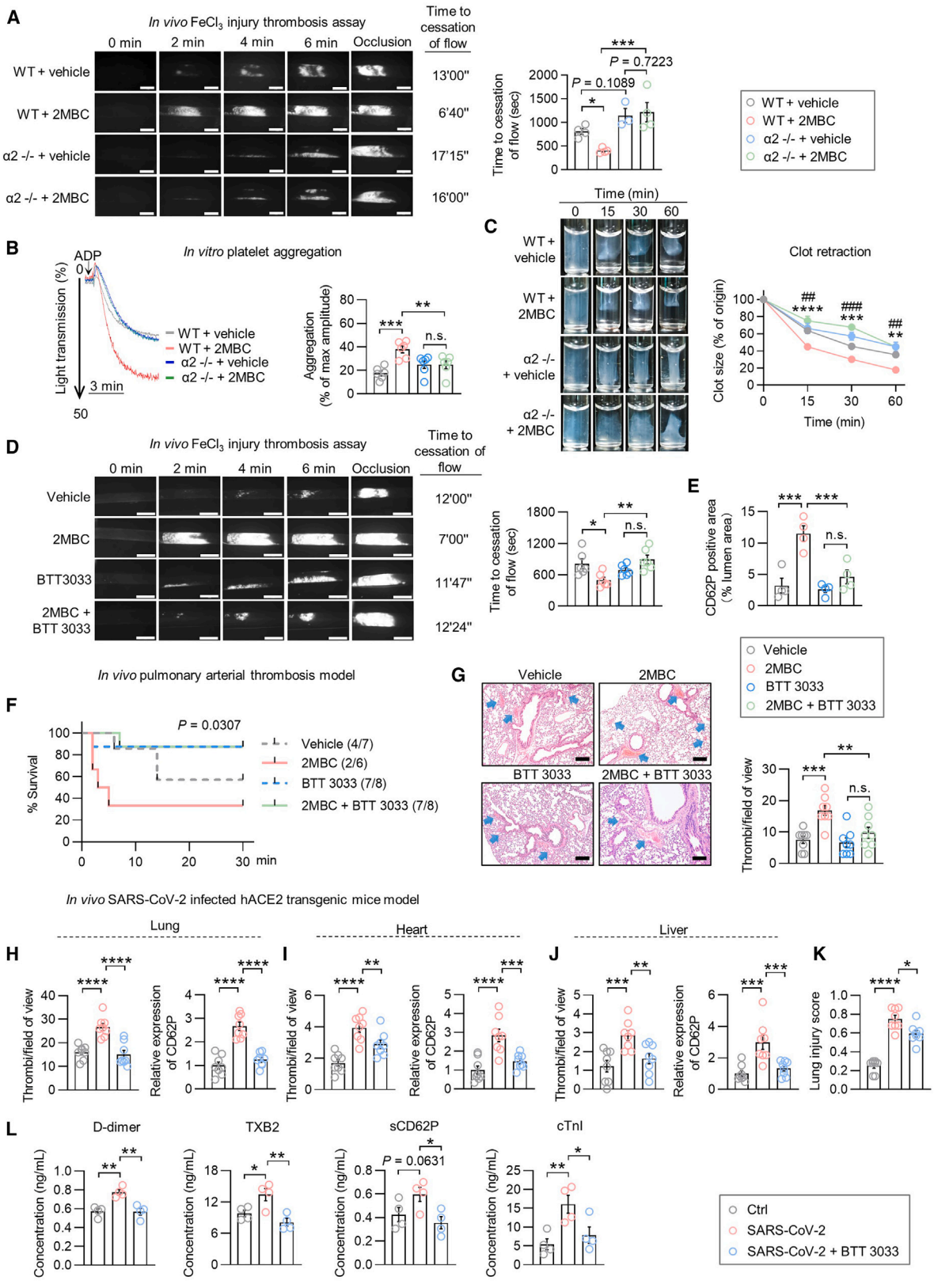

(legend on next page)

Please cite this article in press as: Huang et al., Gut microbial co-metabolite 2-methylbutyrylcarnitine exacerbates thrombosis via binding to and activating integrin α2β1, Cell Metabolism (2024), https://doi.org/10.1016/j.cmet.2024.01.014

metabolic enzymes involved in BCAA catabolism, including *Bcat*, *Bckdh*, *Crat*, *Acad8*, and *Sbcad*, were not altered upon virus infection (Figure S7A). On the other hand, the expression of *Pck1* and *Ace2* was significantly altered after SARS-CoV-2 infection, consistent with our previous report[57] (Figure S7A), suggesting a potential exogenous pathway of 2MBC production under SARS-CoV-2 infection. Alternatively, it was reported that BCAA could be catabolized to 2-methylbutyric acid (2MBA) by bacteria.[58,59] Given the similar chemical structure of 2MBA to 2MBC (Figure 6A), we hypothesized that 2MBA might be a precursor of 2MBC. To investigate whether it may mimic the pro-thrombotic effect of 2MBC *in vivo*, 2MBA was administrated via either oral gavage or i.p. injection. Intriguingly, administration of 2MBA orally, but not i.p., significantly accelerated thrombus formation (Figure 6B). The plasma level of 2MBC was increased by 50% after 2MBA gavage but remained unchanged following i.p. injection of 2MBA (Figure 6C). Unlike 2MBC, 2MBA failed to directly influence platelet function as indicated by *ex vivo* platelet aggregometry assay (Figure 6D). These data suggest that the gut microbiota may be responsible for the 2MBA to 2MBC conversion, and 2MBC may promote thrombosis. Supporting this, refeeding of chow diet after an overnight fast increased the plasma level of 2MBC by approximately 75%, whereas this effect was largely reversed by pre-treatment of antibiotics (Figure 6E).

To further confirm this hypothesis, we performed *in vitro* fecal fermentation and *in vivo* antibiotic intervention. First, we cultured colonic feces collected from C57BL/6J mice and measured 2MBC in the culture medium after incubation with 2MBA. The 2MBC level was increased by nearly 1-fold following 1 h treatment of 2MBA (Figure 6F) and elevated in a time-dependent manner (Figure S7B). In mice, when an antibiotic cocktail was added in drinking water, the presence of the fecal 16S rDNA was almost completely depleted, indicating a nearly complete depletion of the gut microbiota (Figure S7C). The conversion of gavaged 2MBA to 2MBC was strongly inhibited after antibiotic treatment, as indicated by a dramatic reduction of plasma 2MBC levels (Figure 6G). Likewise, pre-treatment of various clinically relevant antibiotics in drinking water exhibited varying suppressing effects on gut microbiota abundance (Figure S7D) and 2MBC generation (Figure S7E). However, utilization of intravenous antibiotics did not affect the plasma 2MBC levels in patients with COVID-19 (Figure S7F), which may be due to their limited influence on the bacteria community in gut (Figures S7G and S7H).[60,61]

To further determine the impact of gut microbiota on platelet function and thrombosis potential via modulating 2MBC levels, a fecal microbiota transplantation (FMT) experiment was conducted. Mice were treated with or without antibiotics and followed by microbial recolonization. Fecal 16S rDNA analysis confirmed that the bacteria count was almost recovered to a comparable level of conventional mice (Figure S7C). Then, mice were gavaged with 2MBA and subsequently subjected to *in vivo* $FeCl_3$-induced thrombosis assay or *ex vivo* platelet aggregometry. The scheme of study design was illustrated in Figure 6H. Consistently, 2MBA gavage markedly increased plasma 2MBC (Figure S7I), leading to exacerbated thrombus formation (Figures 6I and S7J) and platelet aggregation (Figures 6J and S7K). In contrast, antibiotic treatment abrogated the pro-thrombotic effect of 2MBA, which was almost completely recovered after microbial recolonization (Figures 6I, 6J, S7J, and S7K), resembling the alteration pattern of plasma 2MBC (Figure S7I). However, neither antibiotics nor FMT intervention itself exerted effects on platelet aggregation and thrombosis in mice (Figures 6I, 6J, S7J, and S7K). Taken together, our findings clarify that 2MBA could be converted to 2MBC by gut microbiota, and the subsequent 2MBC induces platelet hyperresponsiveness and promotes thrombosis *in vivo*.

Finally, to clarify whether 2MBC is an intermediate metabolite bridging gut microbiota dysbiosis and thrombosis potential in COVID-19, hACE2 mice were pre-treated with antibiotics and then inoculated intranasally with SARS-CoV-2. Notably, plasma 2MBC was increased by approximately 0.5-fold at the 7th day after virus infection, whereas it was almost reversed to a normal level after antibiotic treatment (Figure 6K). Along with that, the heightened platelet reactivity and thrombosis potency were largely suppressed, as indicated by the reduction of CD62P expression in multiple organs including lung, heart, and liver (Figures 6L and S7L). In addition, antibiotic administration showed a slight trend toward an improvement of lung damage following SARS-CoV-2 infection ($p = 0.0621$) (Figure S7M), as well as a reduction in plasma biomarkers related to thrombotic events (D-dimer, TXB2, sCD62p, and cTnI) (Figure 6M). Notably, the concentration of 2MBC was positively correlated with D-dimer ($r = 0.816$, $p = 0.002$), TXB2 ($r = 0.715$, $p = 0.011$), and

Figure 5. Genetic depletion or pharmacological inhibition of integrin α2β1 ameliorates the pro-thrombotic effect of 2MBC

(A) $FeCl_3$-induced carotid artery injury thrombosis assay for integrin α2 knockout (α2−/−) mice or their wild-type littermates (WT) i.p. injected with saline or 100 μg/kg 2MBC (left to right, n = 4, 4, 3, and 4). Scale bars, 500 μm.

(B and C) PRP from α2−/− or WT mice was isolated and incubated with saline or 0.5 μM 2MBC for *in vitro* ADP (5 μM)-stimulated platelet aggregometry (B) and clot retraction assay (C) (n = 3 with 2 technical duplicates).

(D) $FeCl_3$-induced carotid artery injury thrombosis assay for mice i.p. injected with saline or 100 μg/kg 2MBC with or without BTT 3033 (1 mg/kg) (n = 6). Scale bars, 500 μm.

(E) Quantification of CD62P IHC staining of carotid thrombus samples.

(F and G) Pulmonary arterial thrombosis assay for mice i.p. injected with saline or 100 μg/kg 2MBC and with or without BTT 3033 (1 mg/kg). Kaplan-Meier curves (F, n = 7 for vehicle, n = 6 for 2MBC, n = 8 for BTT 3033, and 2MBC + BTT 3033). Representative images of the lung sections and quantifications. Scale bars, 100 μm (G) (n = 4 mice, with two sections per mouse).

(H–L) hACE2 transgenic mice were intranasally inoculated of SARS-CoV-2 or its vehicle, followed by daily i.p. injection of BTT 3033 (1 mg/kg) (n = 4). Quantifications of thrombi numbers and CD62P expression for the lung (H), heart (I), and liver (J) and quantification of lung injury score (K). n = 4 mice per group, two sections per mouse. Related images are shown in Figures S6J–S6L. Plasma D-dimer, TXB2, sCD62P, and cTnI (L).

Data points represent the means ± SEM. Statistics used one-way ANOVA with Fisher's LSD post hoc test (A, B, D, E, G–J, and L), two-way ANOVA with repeated measures (C), log-rank (Mantel-Cox) test (F), or Brown-Forsythe and Welch ANOVA followed by unpaired t test with Welch's correction (K). n.s., not significant; $^{*}p < 0.05$; $^{**,\#\#}p < 0.01$; $^{***,\#\#\#}p < 0.001$; $^{****}p < 0.0001$. For (C), the significance of WT + vehicle versus WT + 2MBC was shown as *, and WT + 2MBC versus α2−/− + 2MBC as #.

Please cite this article in press as: Huang et al., Gut microbial co-metabolite 2-methylbutyrylcarnitine exacerbates thrombosis via binding to and activating integrin α2β1, Cell Metabolism (2024), https://doi.org/10.1016/j.cmet.2024.01.014

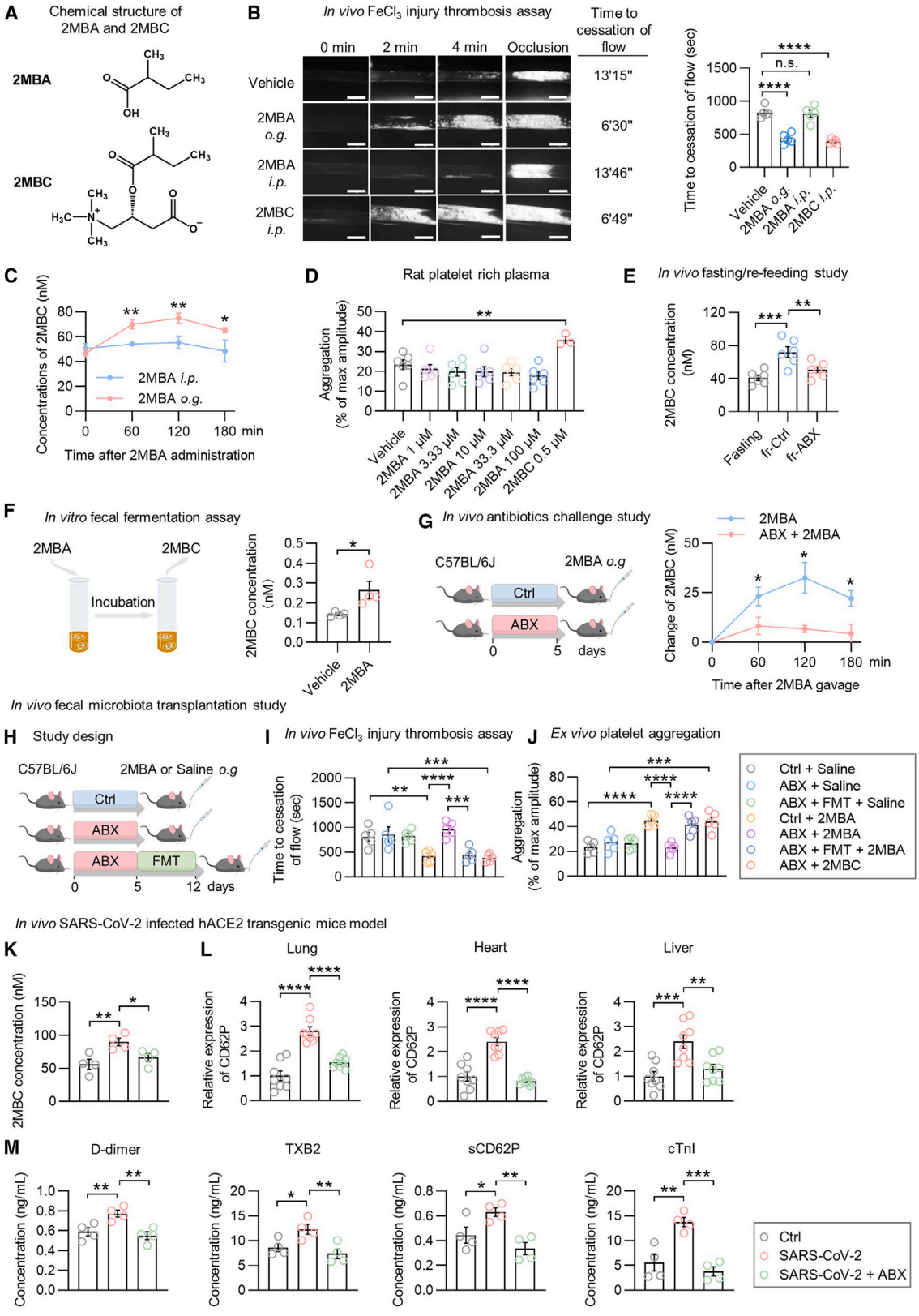

(legend on next page)

Please cite this article in press as: Huang et al., Gut microbial co-metabolite 2-methylbutyrylcarnitine exacerbates thrombosis via binding to and activating integrin α2β1, Cell Metabolism (2024), https://doi.org/10.1016/j.cmet.2024.01.014

cTnI (r = 0.622, p = 0.035), whereas sCD62P represented a similar trend without statistical significance (r = 0.531, p = 0.079) (Figure S7N). Collectively, our data suggest that modulation of gut microbiota ecology may serve as a promising strategy in ameliorating the risk of thrombosis.

DISCUSSION

Thrombosis represents a common pathology underlying ischemic cardiovascular diseases. Our study clarified that 2MBC increases thrombotic risk due to platelet hyperreactivity; mechanistically, 2MBC directly binds to integrin α2β1, which enhances cPLA2 activation and platelet reactivity in response to extracellular stimuli; furthermore, we identified that 2MBC is a host and gut microbial co-metabolite potentially linking gut microbiota dysbiosis and thrombosis (Figure 7).

Unlike most of the acylcarnitine species synthesized during FAO, short branched-chain acylcarnitines are intermediate products of BCAA catabolism.[52] Despite increasing evidence that has implied the associations between short branched-chain acylcarnitines and numerous metabolic disorders including obesity,[27] diabetes,[27,62] non-alcoholic steatohepatitis,[63] and hypertension,[29] the causal role and mechanistic insight have not yet been reported. This study uncovered a biological regulatory effect of 2MBC on thrombotic tendency. 2MBC was abnormally accumulated in both fecal samples and plasma of COVID-19 patients and was positively associated with an increased thrombotic risk. In particular, we demonstrated a robust pro-thrombotic effect of 2MBC by causing platelet hyperreactivity, as indicated by various *in vivo* and *in vitro* thrombosis assays. More importantly, the elevated level of 2MBC did not decline even after a complete clearance of virus in patients with COVID-19, which was in line with a previous metabolomics study in plasma.[64] Our findings unveil a potential mechanism contributing to the increased thrombotic incidence in COVID-19. Additionally, we observed an increased level of plasma 2MBC in patients with ACS and AIS, suggesting a broader relationship between the aberrant accumulation of 2MBC and major adverse consequences of cardiovascular diseases. Notably, an increased plasma level of 2MBC was documented in patients with obesity and diabetes,[27,62] which are of remarkably higher risk for thrombotic events.[65,66] Along with the traditional risk factors, our findings implicated a previously unknown driving factor for increased thrombotic potential in metabolic disorders, such as obesity and diabetes. Taken together, our data clarify 2MBC as a pivotal motivator that aggravated the adverse thrombotic events.

Integrins are surface receptors that mediate cell-cell or cell-matrix interaction. In platelets, integrins play a crucial role in thrombus formation.[67] SPR assay indicated direct binding of 2MBC to integrin α2β1 protein, suggesting a ligand-receptor interaction. More importantly, 2MBC binding appeared to activate signaling cascades downstream of integrin, whereas genetic depletion or pharmacological inhibition of integrin α2β1 largely blocked the pro-thrombotic effects triggered by 2MBC, indicating that integrin α2β1 is an important functional target of 2MBC to regulate platelet reactivity. Thus, 2MBC enhanced platelet responses via potentiating cPLA2 signal activation in an integrin α2β1-dependent manner. We, therefore, revealed a new biological function of 2MBC as a signaling molecule. Indeed, increasing evidence has demonstrated that metabolites not only serve as intermittent substrates in metabolic reactions but also function as signaling molecules to reflect local or systemic metabolism and mediate a wide range of biological processes.[16,25,68] In particular, since the traditional anti-platelet agents, such as aspirin or clopidogrel, are hampered by the side effect of potential bleeding, targeting integrin α2β1 may serve as an alternative strategy due to its mild impact on hemostasis.[69,70] Therefore, our study suggests that integrin α2β1 might be a promising therapeutic target for the prevention of thrombotic events.

While previously known as a product of intracellular BCAA catabolism,[52,54] our study identified 2MBC as a gut microbiota-derived metabolite by using multiple strategies including *in vitro* fecal fermentation, *in vivo* antibiotic challenge, and FMT study. 2MBA, a metabolite generated from BCAA catabolism by bacteria, can be further converted to 2MBC in a gut microbiota-dependent manner. Our data suggested a potential

Figure 6. 2MBC is an intermediate metabolite bridging gut microbiota dysbiosis and thrombotic events

(A) Chemical structure of 2MBA (upper) and 2MBC (lower).

(B) Comparison of the effects of 50 μg/kg 2MBA administration via oral gavage (o.g.) or i.p. injection on thrombus formation following $FeCl_3$-induced carotid artery injury in mice. Mice treated with i.p. injection of 100 μg/kg 2MBC were set as positive control. n = 5; scale bars, 500 μm.

(C) Plasma 2MBC in mice administrated with 50 μg/kg 2MBA via o.g. or i.p. injection (n = 5 biological replicates for 0, 60, and 120 min, and n = 3 for 180 min in each group).

(D) ADP (2 μM)-stimulated platelet aggregometry responses in rat PRP pre-incubated with saline or indicated concentrations of 2MBA (n = 3 with 2 technical repeats) or 2MBC (positive control, n = 3).

(E) Plasma 2MBC following fasting/re-feeding in mice pre-treated with or without antibiotic cocktail. Mice that fasted in the same period without antibiotic treatment or following re-feeding were set as control (n = 6).

(F) Schematic diagram (left) and changes of 2MBC levels in culture medium at 1 h after PBS or 200 μM 2MBA incubation (right) (n = 4).

(G) Changes in plasma 2MBC at the indicated time points following 2MBA o.g. in mice administrated with antibiotic cocktail (versus vehicle) (n = 6).

(H–J) Mice were administrated with antibiotic cocktail and with or without fecal microbial transplantation, then subsequently administrated with saline or 50 μg/kg 2MBA via o.g. Mice i.p. injection with 100 μg/kg 2MBC were set as positive control (n = 5). Schematic diagram of study design (H). Quantifications of occlusive thrombosis time (I). ADP (5 μM)-stimulated platelet aggregometry responses in mice PRP (J).

(K–M) hACE2 transgenic mice treated with antibiotics cocktail were intranasally inoculated of SARS-CoV-2 or its vehicle (n = 4). 2MBC concentrations in plasma (K). Quantifications of relative CD62P expression of IHC staining for the lung, heart, and liver. Two sections per mouse (L). Plasma D-dimer, TXB2, sCD62P, and cTnI (M).

Data points represent the means ± SEM. Statistics used one-way ANOVA with Fisher's LSD post hoc test (B, E, and I–M), Brown-Forsythe and Welch ANOVA followed by unpaired t test with Welch's correction (D and N), unpaired Student's t test (F), or two-way ANOVA with repeated measures (C and G). n.s., not significant; *p < 0.05; **p < 0.01; ***p < 0.001; ****p < 0.0001. For (I), (J), and (L), images are shown in Figures S7J–S7L.

Please cite this article in press as: Huang et al., Gut microbial co-metabolite 2-methylbutyrylcarnitine exacerbates thrombosis via binding to and activating integrin α2β1, Cell Metabolism (2024), https://doi.org/10.1016/j.cmet.2024.01.014

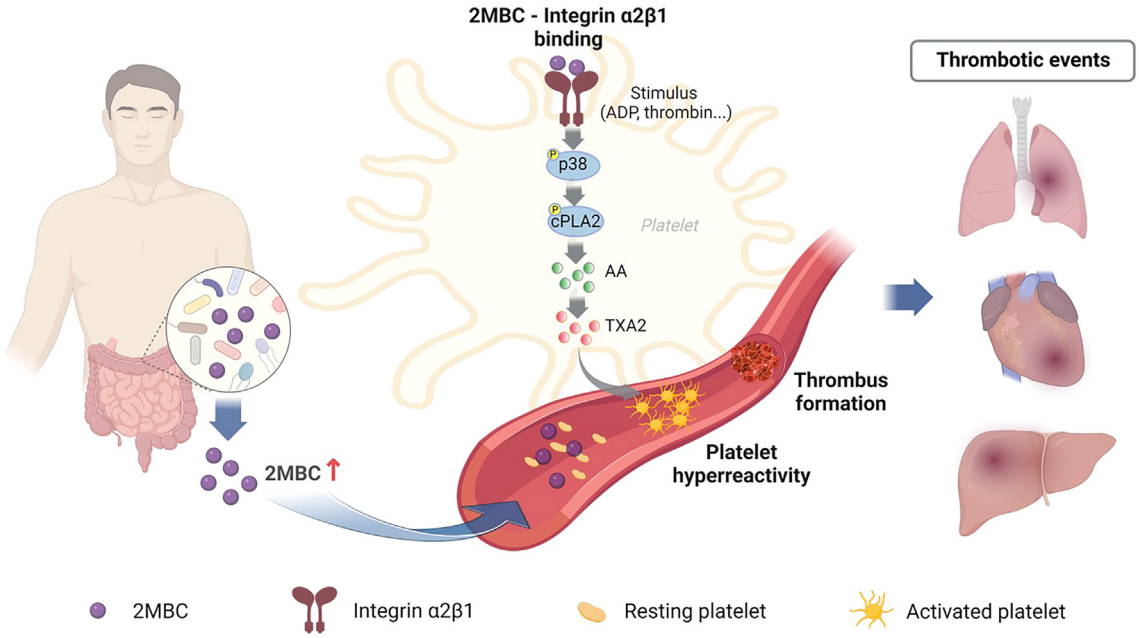

Figure 7. Summary scheme illustrating gut microbial co-metabolite 2MBC exacerbates thrombosis via binding to and potentiating integrin α2β1 activation

Gut microbiota dysbiosis leads to abnormal accumulation of circulating 2MBC. 2MBC directly binds to and potentiates integrin α2β1 activation in platelet under the stimulation of agonists, which promotes cPLA2-mediated TXA2 generation and platelet hyperresponsiveness, thus increasing the thrombotic tendency in the host. Figure was created with Biorender.com.

causality of 2MBC accumulation with the dysbiosis of gut microbiota. In consonance with our finding, western dietary pattern with great impact on gut microbial composition[71] was associated with a higher plasma concentration of 2MBC.[72] In fact, gut microbiota-derived metabolites could serve as an intermediate that mediates the effect of gut microbiota dysbiosis on MACEs.[14,16,73] Targeting gut microbial community to normalize the elevated levels of pathogenic metabolites may represent a promising therapeutic strategy.[15,74,75] Supporting this, we found that increased plasma 2MBC levels, as well as the heightened thrombosis tendency upon SARS-CoV-2 infection, were remarkably suppressed after elimination of gut microbiota by antibiotic cocktail. Collectively, our findings suggest that modulation of gut microbiota ecology may represent a promising strategy in ameliorating the thrombosis potential secondary to 2MBC accumulation.

In summary, our findings identified 2MBC as an intermediate metabolite linking gut microbiota dysbiosis and an increased risk for thrombosis, providing new mechanistic insight and a potential therapeutic strategy for thrombotic events.

Limitations of the study

First, plasma endotoxin activity and lipopolysaccharide concentration were increased in patients with COVID-19,[76,77] suggesting the potential enhanced intestinal permeability. However, whether it may facilitate intestinal 2MBC translocation in circulation remains elusive. Second, although we documented integrin α2β1 as the cellular target for 2MBC, some other targets may exist in cells and remain to be explored.

STAR★METHODS

Detailed methods are provided in the online version of this paper and include the following:

- KEY RESOURCES TABLE
- RESOURCE AVAILABILITY
  - Lead contact
  - Materials availability
  - Data and code availability
- EXPERIMENTAL MODEL AND SUBJECT DETAILS
  - COVID-19 Subjects and Study Design
  - Blood Collection
  - Animal Studies
  - Cell Culture
  - Platelet Rich Plasma or Washed Platelet Isolation from Human Donors
  - Platelet Rich Plasma or Washed Platelet Isolation from Rodent
- METHOD DETAILS
  - Untargeted Liquid Chromatography-Mass Spectrometry (LC-MS/MS) Analysis
  - Targeted LC-MS/MS Analysis
  - 16S rDNA Sequencing
  - Carotid Artery $FeCl_3$ Injury Thrombosis Assay
  - Photochemical Injury Thrombosis Assay
  - Thrombin Induced Pulmonary Artery Thrombosis Assay
  - Echocardiography

SUPPLEMENTAL INFORMATION

Supplemental information can be found online at https://doi.org/10.1016/j.cmet.2024.01.014.

ACKNOWLEDGMENTS

This work is supported by grants from The National Natural Science Foundation of China (no. 32271185), The National Outstanding Youth Science Fund Project of National Natural Science Foundation of China (no. 82222014), Guangzhou Science and Technology Program Key Projects (no. 202206010031), Guangdong Science and Technology Department (no. 2023B1212060013), Guangdong Clinical Research Center for Metabolic Diseases (no. 2020B1111170009), Guangzhou Key Laboratory for Metabolic Diseases (no. 202102100004), and Science and Technology Program of Guangdong Province (no. 2021B1212030016). We thank Xuanhong Zhang (Core Facilities for Medical Science, Zhongshan School of Medicine, Sun Yat-sen University) for technical support during the surface plasmon resonance study. We also thank Qiao Su (Animal Center, The First Affiliated Hospital of Sun Yat-Sen University) for technical support during *in vivo* studies. Mass spectrometry and phosphoproteomics analysis were performed by the Bioinformatics and Omics Center, Sun Yat-sen Memorial Hospital, Sun Yat-sen University, and Wuhan Metware Biotechnology. *In silico* virtual docking simulation was performed using VSTH (https://matgen.nscc-gz.cn/VirtualScreening.html).

AUTHOR CONTRIBUTIONS

K.H., Z.L., X. He, D.F., Zefeng Zhang, Y. Liu, N.L., Zhongyu Zhang, J.P., C.L., R.Z., Z.C., T.W., W.Y., P.L., Liyan Lin, J. Wen, Zhengde Zhao, X. Huang, L. Yuan, L. Zhou, H.W., L.H., Lin Lin, and Y. Luo performed the experiments. J.D., Y.S., S.Y., L. Zhang, D.H., and S.H. performed *in vivo* SARS-CoV-2 infection experiments. B.H. and Jingyu Li contributed to bioinformatics analysis. K.H., Z.L., X. He, J.D., B.H., Y.S., D.F., Zefeng Zhang, Y. Liu, and N.L. acquired, interpreted, and analyzed the data. K.H., Z.L., M.R., and S.C. wrote and edited the manuscript with input from all authors. M.C. performed targeted metabolomics analysis. P.C. contributed *in silico* virtual docking simulation. Linghua Li, K.F., J. Wang, B.L., Weiping Cai, X.D., Y. Li, Jianping Li, Z.H., L. Yang, Jiaojiao Li, Y. Zhuo, and F.Z. contributed to clinical data and samples from COVID-19 cohort. W.Z., Q.N., and X. Hong helped with untargeted metabolomics analysis from the COVID-19 cohort. Linghua Li, M.R., L. Yan, F.L., Y. Lu, Weikang Cai, D.G., Y. Zhang, and G.C. provided critical scientific input and discussion. S.C. conceived, designed, and supervised the entire project. All authors contributed to the critical review of the manuscript.

DECLARATION OF INTERESTS

The authors declare no competing interests.

Received: May 24, 2023
Revised: November 8, 2023
Accepted: January 25, 2024
Published: February 23, 2024

REFERENCES

1. Angiolillo, D.J., Bernardo, E., Sabaté, M., Jimenez-Quevedo, P., Costa, M.A., Palazuelos, J., Hernández-Antolin, R., Moreno, R., Escaned, J., Alfonso, F., et al. (2007). Impact of platelet reactivity on cardiovascular outcomes in patients with type 2 diabetes mellitus and coronary artery disease. J. Am. Coll. Cardiol. *50*, 1541–1547.
2. Puurunen, M.K., Hwang, S.J., Larson, M.G., Vasan, R.S., O'Donnell, C.J., Tofler, G., and Johnson, A.D. (2018). ADP platelet hyperreactivity predicts cardiovascular disease in the FHS (Framingham Heart Study). J. Am. Heart Assoc. *7*, e008522.
3. Gremmel, T., Steiner, S., Seidinger, D., Koppensteiner, R., Panzer, S., and Kopp, C.W. (2013). Obesity is associated with poor response to clopidogrel and an increased susceptibility to protease activated receptor-1 mediated platelet activation. Transl. Res. *161*, 421–429.
4. Biswas, S., Zimman, A., Gao, D., Byzova, T.V., and Podrez, E.A. (2017). TLR2 plays a key role in platelet hyperreactivity and accelerated thrombosis associated with hyperlipidemia. Circ. Res. *121*, 951–962.
5. Zhao, W., Wei, Z., Xin, G., Li, Y., Yuan, J., Ming, Y., Ji, C., Sun, Q., Li, S., Chen, X., et al. (2021). Piezo1 initiates platelet hyperreactivity and accelerates thrombosis in hypertension. J. Thromb. Haemost. *19*, 3113–3125.
6. Shen, Y.M., and Frenkel, E.P. (2004). Thrombosis and a hypercoagulable state in HIV-infected patients. Clin. Appl. Thromb. Hemost. *10*, 277–280.
7. Voss, E.A., Shoaibi, A., Yin Hui Lai, L., Blacketer, C., Alshammari, T., Makadia, R., Haynes, K., Sena, A.G., Rao, G., van Sandijk, S., et al. (2023). Contextualising adverse events of special interest to characterise the baseline incidence rates in 24 million patients with COVID-19 across 26 databases: a multinational retrospective cohort study. EClinicalMedicine *58*, 101932.
8. Giannis, D., Allen, S.L., Tsang, J., Flint, S., Pinhasov, T., Williams, S., Tan, G., Thakur, R., Leung, C., Snyder, M., et al. (2021). Postdischarge thromboembolic outcomes and mortality of hospitalized patients with COVID-19: the CORE-19 registry. Blood *137*, 2838–2847.
9. Knight, R., Walker, V., Ip, S., Cooper, J.A., Bolton, T., Keene, S., Denholm, R., Akbari, A., Abbasizanjani, H., Torabi, F., et al. (2022). Association of COVID-19 with major arterial and venous thrombotic diseases: a population-wide cohort study of 48 million adults in England and Wales. Circulation *146*, 892–906.
10. Manne, B.K., Denorme, F., Middleton, E.A., Portier, I., Rowley, J.W., Stubben, C., Petrey, A.C., Tolley, N.D., Guo, L., Cody, M., et al. (2020). Platelet gene expression and function in patients with COVID-19. Blood *136*, 1317–1329.
11. Kruger, A., Vlok, M., Turner, S., Venter, C., Laubscher, G.J., Kell, D.B., and Pretorius, E. (2022). Proteomics of fibrin amyloid microclots in long COVID/post-acute sequelae of COVID-19 (PASC) shows many entrapped pro-inflammatory molecules that may also contribute to a failed fibrinolytic system. Cardiovasc. Diabetol. *21*, 190.
12. Skye, S.M., Zhu, W., Romano, K.A., Guo, C.J., Wang, Z., Jia, X., Kirsop, J., Haag, B., Lang, J.M., DiDonato, J.A., et al. (2018). Microbial transplantation with human gut commensals containing CutC is sufficient to transmit enhanced platelet reactivity and thrombosis potential. Circ. Res. *123*, 1164–1176.
13. Kiouptsi, K., Jäckel, S., Pontarollo, G., Grill, A., Kuijpers, M.J.E., Wilms, E., Weber, C., Sommer, F., Nagy, M., Neideck, C., et al. (2019). The microbiota promotes arterial thrombosis in low-density lipoprotein receptor-deficient mice. mBio *10*, e02298-19.

14. Zhu, W., Gregory, J.C., Org, E., Buffa, J.A., Gupta, N., Wang, Z., Li, L., Fu, X., Wu, Y., Mehrabian, M., et al. (2016). Gut microbial metabolite TMAO enhances platelet hyperreactivity and thrombosis risk. Cell *165*, 111–124.
15. Roberts, A.B., Gu, X., Buffa, J.A., Hurd, A.G., Wang, Z., Zhu, W., Gupta, N., Skye, S.M., Cody, D.B., Levison, B.S., et al. (2018). Development of a gut microbe-targeted nonlethal therapeutic to inhibit thrombosis potential. Nat. Med. *24*, 1407–1417.
16. Nemet, I., Saha, P.P., Gupta, N., Zhu, W., Romano, K.A., Skye, S.M., Cajka, T., Mohan, M.L., Li, L., Wu, Y., et al. (2020). A cardiovascular disease-linked gut microbial metabolite acts via adrenergic receptors. Cell *180*, 862–877.e22.
17. Witkowski, M., Witkowski, M., Friebel, J., Buffa, J.A., Li, X.S., Wang, Z., Sangwan, N., Li, L., DiDonato, J.A., Tizian, C., et al. (2022). Vascular endothelial tissue factor contributes to trimethylamine N-oxide-enhanced arterial thrombosis. Cardiovasc. Res. *118*, 2367–2384.
18. Zuo, T., Zhang, F., Lui, G.C.Y., Yeoh, Y.K., Li, A.Y.L., Zhan, H., Wan, Y., Chung, A.C.K., Cheung, C.P., Chen, N., et al. (2020). Alterations in gut microbiota of patients with COVID-19 during time of hospitalization. Gastroenterology *159*, 944–955.e8.
19. Liu, Q., Mak, J.W.Y., Su, Q., Yeoh, Y.K., Lui, G.C., Ng, S.S.S., Zhang, F., Li, A.Y.L., Lu, W., Hui, D.S., et al. (2022). Gut microbiota dynamics in a prospective cohort of patients with post-acute COVID-19 syndrome. Gut *71*, 544–552.
20. Su, Q., Lau, R.I., Liu, Q., Chan, F.K.L., and Ng, S.C. (2023). Post-acute COVID-19 syndrome and gut dysbiosis linger beyond 1 year after SARS-CoV-2 clearance. Gut *72*, 1230–1232.
21. Fan, Y., and Pedersen, O. (2021). Gut microbiota in human metabolic health and disease. Nat. Rev. Microbiol. *19*, 55–71.
22. Qin, J., Li, Y., Cai, Z., Li, S., Zhu, J., Zhang, F., Liang, S., Zhang, W., Guan, Y., Shen, D., et al. (2012). A metagenome-wide association study of gut microbiota in type 2 diabetes. Nature *490*, 55–60.
23. Wu, H., Tremaroli, V., Schmidt, C., Lundqvist, A., Olsson, L.M., Krämer, M., Gummesson, A., Perkins, R., Bergström, G., and Bäckhed, F. (2020). The gut microbiota in prediabetes and diabetes: a population-based cross-sectional study. Cell Metab. *32*, 379–390.e3.
24. Nagata, N., Takeuchi, T., Masuoka, H., Aoki, R., Ishikane, M., Iwamoto, N., Sugiyama, M., Suda, W., Nakanishi, Y., Terada-Hirashima, J., et al. (2023). Human gut microbiota and its metabolites impact immune responses in COVID-19 and its complications. Gastroenterology *164*, 272–288.
25. Krautkramer, K.A., Fan, J., and Bäckhed, F. (2021). Gut microbial metabolites as multi-kingdom intermediates. Nat. Rev. Microbiol. *19*, 77–94.
26. Shen, B., Yi, X., Sun, Y., Bi, X., Du, J., Zhang, C., Quan, S., Zhang, F., Sun, R., Qian, L., et al. (2020). Proteomic and metabolomic characterization of COVID-19 patient sera. Cell *182*, 59–72.e15.
27. Mihalik, S.J., Goodpaster, B.H., Kelley, D.E., Chace, D.H., Vockley, J., Toledo, F.G., and DeLany, J.P. (2010). Increased levels of plasma acylcarnitines in obesity and type 2 diabetes and identification of a marker of glucolipotoxicity. Obesity (Silver Spring) *18*, 1695–1700.
28. Scarale, M.G., Mastroianno, M., Prehn, C., Copetti, M., Salvemini, L., Adamski, J., De Cosmo, S., Trischitta, V., and Menzaghi, C. (2022). Circulating metabolites associate with and improve the prediction of all-cause mortality in type 2 diabetes. Diabetes *71*, 1363–1370.
29. Shi, M., He, J., Li, C., Lu, X., He, W.J., Cao, J., Chen, J., Chen, J.C., Bazzano, L.A., Li, J.X., et al. (2022). Metabolomics study of blood pressure salt-sensitivity and hypertension. Nutr. Metab. Cardiovasc. Dis. *32*, 1681–1692.
30. Hobohm, L., Sagoschen, I., Barco, S., Farmakis, I.T., Fedeli, U., Koelmel, S., Gori, T., Espinola-Klein, C., Münzel, T., Konstantinides, S., and Keller, K. (2023). COVID-19 infection and its impact on case fatality in patients with pulmonary embolism. Eur. Respir. J. *61*, 2200619.
31. Kattula, S., Sang, Y., de Ridder, G., Silver, A.C., Bouck, E.G., Cooley, B.C., and Wolberg, A.S. (2021). Novel venous thromboembolism mouse model to evaluate the role of complete and partial factor XIII deficiency in pulmonary embolism risk. J. Thromb. Haemost. *19*, 2997–3007.
32. Diaz, J.A., Saha, P., Cooley, B., Palmer, O.R., Grover, S.P., Mackman, N., Wakefield, T.W., Henke, P.K., Smith, A., and Lal, B.K. (2019). Choosing a mouse model of venous thrombosis. Arterioscler. Thromb. Vasc. Biol. *39*, 311–318.
33. Al-Samkari, H., Karp Leaf, R.S., Dzik, W.H., Carlson, J.C.T., Fogerty, A.E., Waheed, A., Goodarzi, K., Bendapudi, P.K., Bornikova, L., Gupta, S., et al. (2020). COVID-19 and coagulation: bleeding and thrombotic manifestations of SARS-CoV-2 infection. Blood *136*, 489–500.
34. Stark, K., and Massberg, S. (2021). Interplay between inflammation and thrombosis in cardiovascular pathology. Nat. Rev. Cardiol. *18*, 666–682.
35. Smith, J.B., Araki, H., and Lefer, A.M. (1980). Thromboxane A2, prostacyclin and aspirin: effects on vascular tone and platelet aggregation. Circulation *62*, V19–V25.
36. Nakahata, N. (2008). Thromboxane A2: physiology/pathophysiology, cellular signal transduction and pharmacology. Pharmacol. Ther. *118*, 18–35.
37. Cheng, Y., Austin, S.C., Rocca, B., Koller, B.H., Coffman, T.M., Grosser, T., Lawson, J.A., and FitzGerald, G.A. (2002). Role of prostacyclin in the cardiovascular response to thromboxane A2. Science *296*, 539–541.
38. Adler, D.H., Cogan, J.D., Phillips, J.A., 3rd, Schnetz-Boutaud, N., Milne, G.L., Iverson, T., Stein, J.A., Brenner, D.A., Morrow, J.D., Boutaud, O., and Oates, J.A. (2008). Inherited human cPLA(2alpha) deficiency is associated with impaired eicosanoid biosynthesis, small intestinal ulceration, and platelet dysfunction. J. Clin. Invest. *118*, 2121–2131.
39. Estevez, B., Stojanovic-Terpo, A., Delaney, M.K., O'Brien, K.A., Berndt, M.C., Ruan, C., and Du, X. (2013). LIM kinase-1 selectively promotes glycoprotein Ib-IX-mediated TXA2 synthesis, platelet activation, and thrombosis. Blood *121*, 4586–4594.
40. Schooneman, M.G., Vaz, F.M., Houten, S.M., and Soeters, M.R. (2013). Acylcarnitines: reflecting or inflicting insulin resistance? Diabetes *62*, 1–8.
41. Kulkarni, P.P., Ekhlak, M., Singh, V., Kailashiya, V., Singh, N., and Dash, D. (2023). Fatty acid oxidation fuels agonist-induced platelet activation and thrombus formation: targeting beta-oxidation of fatty acids as an effective anti-platelet strategy. FASEB J. *37*, e22768.
42. Szklarczyk, D., Gable, A.L., Nastou, K.C., Lyon, D., Kirsch, R., Pyysalo, S., Doncheva, N.T., Legeay, M., Fang, T., Bork, P., et al. (2021). The STRING database in 2021: customizable protein-protein networks, and functional characterization of user-uploaded gene/measurement sets. Nucleic Acids Res. *49*, D605–D612.
43. Shattil, S.J., Kashiwagi, H., and Pampori, N. (1998). Integrin signaling: the platelet paradigm. Blood *91*, 2645–2657.
44. Inoue, O., Suzuki-Inoue, K., Dean, W.L., Frampton, J., and Watson, S.P. (2003). Integrin alpha2beta1 mediates outside-in regulation of platelet spreading on collagen through activation of Src kinases and PLCgamma2. J. Cell Biol. *160*, 769–780.
45. Huang, J., Li, X., Shi, X., Zhu, M., Wang, J., Huang, S., Huang, X., Wang, H., Li, L., Deng, H., et al. (2019). Platelet integrin αIIbβ3: signal transduction, regulation, and its therapeutic targeting. J. Hematol. Oncol. *12*, 26.
46. Léon, C., Freund, M., Ravanat, C., Baurand, A., Cazenave, J.P., and Gachet, C. (2001). Key role of the P2Y(1) receptor in tissue factor-induced thrombin-dependent acute thromboembolism: studies in P2Y(1)-knockout mice and mice treated with a P2Y(1) antagonist. Circulation *103*, 718–723.
47. Zhang, Y., Ehrlich, S.M., Zhu, C., and Du, X. (2022). Signaling mechanisms of the platelet glycoprotein Ib-IX complex. Platelets *33*, 823–832.
48. Mo, Q., Xu, Z., Yan, H., Chen, P., and Lu, Y. (2023). VSTH: a user-friendly web server for structure-based virtual screening on Tianhe-2. Bioinformatics *39*, btac740.
49. Mitra, S.K., and Schlaepfer, D.D. (2006). Integrin-regulated FAK-Src signaling in normal and cancer cells. Curr. Opin. Cell Biol. *18*, 516–523.
50. Marjoram, R.J., Li, Z., He, L., Tollefsen, D.M., Kunicki, T.J., Dickeson, S.K., Santoro, S.A., and Zutter, M.M. (2014). alpha2beta1 integrin, GPVI receptor, and common FcRgamma chain on mouse platelets mediate distinct responses to collagen in models of thrombosis. PLoS One *9*, e114035.

51. Nissinen, L., Koivunen, J., Käpylä, J., Salmela, M., Nieminen, J., Jokinen, J., Sipilä, K., Pihlavisto, M., Pentikäinen, O.T., Marjamäki, A., and Heino, J. (2012). Novel alpha2beta1 integrin inhibitors reveal that integrin binding to collagen under shear stress conditions does not require receptor preactivation. J. Biol. Chem. *287*, 44694–44702.

52. Roe, D.S., Roe, C.R., Brivet, M., and Sweetman, L. (2000). Evidence for a short-chain carnitine-acylcarnitine translocase in mitochondria specifically related to the metabolism of branched-chain amino acids. Mol. Genet. Metab. *69*, 69–75.

53. Violante, S., Ijlst, L., Ruiter, J., Koster, J., van Lenthe, H., Duran, M., de Almeida, I.T., Wanders, R.J., Houten, S.M., and Ventura, F.V. (2013). Substrate specificity of human carnitine acetyltransferase: implications for fatty acid and branched-chain amino acid metabolism. Biochim. Biophys. Acta *1832*, 773–779.

54. McCalley, S., Pirman, D., Clasquin, M., Johnson, K., Jin, S., and Vockley, J. (2019). Metabolic analysis reveals evidence for branched chain amino acid catabolism crosstalk and the potential for improved treatment of organic acidurias. Mol. Genet. Metab. *128*, 57–61.

55. Wang, J., Liu, Y., Lian, K., Shentu, X., Fang, J., Shao, J., Chen, M., Wang, Y., Zhou, M., and Sun, H. (2019). BCAA catabolic defect alters glucose metabolism in lean mice. Front. Physiol. *10*, 1140.

56. Rossi, A., Turturo, M., Albano, L., Fecarotta, S., Barretta, F., Crisci, D., Gallo, G., Perfetto, R., Uomo, F., Vallone, F., et al. (2022). Long-term monitoring for short/branched-chain acyl-CoA dehydrogenase deficiency: a single-center 4-year experience and open issues. Front. Pediatr. *10*, 895921.

57. Li, Z., Peng, M., Chen, P., Liu, C., Hu, A., Zhang, Y., Peng, J., Liu, J., Li, Y., Li, W., et al. (2022). Imatinib and methazolamide ameliorate COVID-19-induced metabolic complications via elevating ACE2 enzymatic activity and inhibiting viral entry. Cell Metab. *34*, 424–440.e7.

58. Madsen, S.M., Beck, H.C., Ravn, P., Vrang, A., Hansen, A.M., and Israelsen, H. (2002). Cloning and inactivation of a branched-chain-amino-acid aminotransferase gene from Staphylococcus carnosus and characterization of the enzyme. Appl. Environ. Microbiol. *68*, 4007–4014.

59. Ganesan, B., Dobrowolski, P., and Weimer, B.C. (2006). Identification of the leucine-to-2-methylbutyric acid catabolic pathway of Lactococcus lactis. Appl. Environ. Microbiol. *72*, 4264–4273.

60. Kelly, S.A., Nzakizwanayo, J., Rodgers, A.M., Zhao, L., Weiser, R., Tekko, I.A., McCarthy, H.O., Ingram, R.J., Jones, B.V., Donnelly, R.F., and Gilmore, B.F. (2021). Antibiotic therapy and the gut microbiome: investigating the effect of delivery route on gut pathogens. ACS Infect. Dis. *7*, 1283–1296.

61. Xue, L., Ding, Y., Qin, Q., Liu, L., Ding, X., Zhou, Y., Liu, K., Singla, R.K., Shen, K., Din, A.U., et al. (2022). Assessment of the impact of intravenous antibiotics treatment on gut microbiota in patients: clinical data from pre- and post-cardiac surgery. Front. Cell. Infect. Microbiol. *12*, 1043971.

62. Sun, L., Liang, L., Gao, X., Zhang, H., Yao, P., Hu, Y., Ma, Y., Wang, F., Jin, Q., Li, H., et al. (2016). Early prediction of developing type 2 diabetes by plasma acylcarnitines: a population-based study. Diabetes Care *39*, 1563–1570.

63. Kalhan, S.C., Guo, L., Edmison, J., Dasarathy, S., McCullough, A.J., Hanson, R.W., and Milburn, M. (2011). Plasma metabolomic profile in nonalcoholic fatty liver disease. Metabolism *60*, 404–413.

64. Wu, J., Zhao, M., Li, C., Zhang, Y., and Wang, D.W. (2021). The SARS-CoV-2 induced targeted amino acid profiling in patients at hospitalized and convalescent stage. Biosci. Rep. *41*, BSR20204201.

65. Larsson, S.C., Bäck, M., Rees, J.M.B., Mason, A.M., and Burgess, S. (2020). Body mass index and body composition in relation to 14 cardiovascular conditions in UK Biobank: a Mendelian randomization study. Eur. Heart J. *41*, 221–226.

66. Joseph, J.J., Deedwania, P., Acharya, T., Aguilar, D., Bhatt, D.L., Chyun, D.A., Di Palo, K.E., Golden, S.H., and Sperling, L.S.; American Heart Association Diabetes Committee of the Council on Lifestyle and Cardiometabolic Health; Council on Arteriosclerosis, Thrombosis and Vascular Biology; Council on Clinical Cardiology; and Council on Hypertension (2022). Comprehensive management of cardiovascular risk factors for adults with type 2 diabetes: a scientific statement from the American Heart Association. Circulation *145*, e722–e759.

67. He, L., Pappan, L.K., Grenache, D.G., Li, Z., Tollefsen, D.M., Santoro, S.A., and Zutter, M.M. (2003). The contributions of the alpha 2 beta 1 integrin to vascular thrombosis in vivo. Blood *102*, 3652–3657.

68. Cohen, L.J., Esterhazy, D., Kim, S.H., Lemetre, C., Aguilar, R.R., Gordon, E.A., Pickard, A.J., Cross, J.R., Emiliano, A.B., Han, S.M., et al. (2017). Commensal bacteria make GPCR ligands that mimic human signalling molecules. Nature *549*, 48–53.

69. Nieswandt, B., Brakebusch, C., Bergmeier, W., Schulte, V., Bouvard, D., Mokhtari-Nejad, R., Lindhout, T., Heemskerk, J.W., Zirngibl, H., and Fässler, R. (2001). Glycoprotein VI but not alpha2beta1 integrin is essential for platelet interaction with collagen. EMBO J. *20*, 2120–2130.

70. Holtkötter, O., Nieswandt, B., Smyth, N., Müller, W., Hafner, M., Schulte, V., Krieg, T., and Eckes, B. (2002). Integrin alpha 2-deficient mice develop normally, are fertile, but display partially defective platelet interaction with collagen. J. Biol. Chem. *277*, 10789–10794.

71. Sonnenburg, E.D., Smits, S.A., Tikhonov, M., Higginbottom, S.K., Wingreen, N.S., and Sonnenburg, J.L. (2016). Diet-induced extinctions in the gut microbiota compound over generations. Nature *529*, 212–215.

72. Bhupathiraju, S.N., Guasch-Ferré, M., Gadgil, M.D., Newgard, C.B., Bain, J.R., Muehlbauer, M.J., Ilkayeva, O.R., Scholtens, D.M., Hu, F.B., Kanaya, A.M., and Kandula, N.R. (2018). Dietary patterns among Asian Indians living in the United States have distinct metabolomic profiles that are associated with cardiometabolic risk. J. Nutr. *148*, 1150–1159.

73. Zhu, W., Romano, K.A., Li, L., Buffa, J.A., Sangwan, N., Prakash, P., Tittle, A.N., Li, X.S., Fu, X., Androjna, C., et al. (2021). Gut microbes impact stroke severity via the trimethylamine N-oxide pathway. Cell Host Microbe *29*, 1199–1208.e5.

74. Chakaroun, R.M., Olsson, L.M., and Bäckhed, F. (2023). The potential of tailoring the gut microbiome to prevent and treat cardiometabolic disease. Nat. Rev. Cardiol. *20*, 217–235.

75. Schupack, D.A., Mars, R.A.T., Voelker, D.H., Abeykoon, J.P., and Kashyap, P.C. (2022). The promise of the gut microbiome as part of individualized treatment strategies. Nat. Rev. Gastroenterol. Hepatol. *19*, 7–25.

76. Dela Cruz, P.T.H., Davison, D., Yamane, D.P., Chu, E., and Seneff, M. (2023). Increased endotoxin activity in COVID-19 patients admitted to the intensive care unit. J. Intensive Care Med. *38*, 27–31.

77. Teixeira, P.C., Dorneles, G.P., Santana Filho, P.C., da Silva, I.M., Schipper, L.L., Postiga, I.A.L., Neves, C.A.M., Rodrigues Junior, L.C., Peres, A., Souto, J.T., et al. (2021). Increased LPS levels coexist with systemic inflammation and result in monocyte activation in severe COVID-19 patients. Int. Immunopharmacol. *100*, 108125.

78. Xu, Y., Chen, Y., and Tang, X. (2020). Guidelines for the diagnosis and treatment of coronavirus disease 2019 (COVID-19) in China. Glob. Health Med. *2*, 66–72.

79. Huang, K., Liu, C., Peng, M., Su, Q., Liu, R., Guo, Z., Chen, S., Li, Z., and Chang, G. (2021). Glycoursodeoxycholic acid ameliorates atherosclerosis and alters gut microbiota in apolipoprotein E-deficient mice. J. Am. Heart Assoc. *10*, e019820.

80. Thibault, H.B., Kurtz, B., Raher, M.J., Shaik, R.S., Waxman, A., Derumeaux, G., Halpern, E.F., Bloch, K.D., and Scherrer-Crosbie, M. (2010). Noninvasive assessment of murine pulmonary arterial pressure: validation and application to models of pulmonary hypertension. Circ. Cardiovasc. Imaging *3*, 157–163.

81. Sun, L., Xie, C., Wang, G., Wu, Y., Wu, Q., Wang, X., Liu, J., Deng, Y., Xia, J., Chen, B., et al. (2018). Gut microbiota and intestinal FXR mediate the clinical benefits of metformin. Nat. Med. *24*, 1919–1929.

82. Kulkarni, H.S., Lee, J.S., Bastarache, J.A., Kuebler, W.M., Downey, G.P., Albaiceta, G.M., Altemeier, W.A., Artigas, A., Bates, J.H.T., Calfee, C.S., et al. (2022). Update on the features and measurements of experimental acute lung injury in animals: an official American Thoracic Society Workshop report. Am. J. Respir. Cell Mol. Biol. *66*, e1–e14.

83. Wei, G., Xu, X., Tong, H., Wang, X., Chen, Y., Ding, Y., Zhang, S., Ju, W., Fu, C., Li, Z., et al. (2020). Salidroside inhibits platelet function and thrombus formation through AKT/GSK3beta signaling pathway. Aging (Albany, NY) *12*, 8151–8166.

84. Hassan, M.M., Sharmin, S., Kim, H.J., and Hong, S.T. (2021). Identification and characterization of plasmin-independent thrombolytic enzymes. Circ. Res. *128*, 386–400.

85. He, X., Liu, C., Peng, J., Li, Z., Li, F., Wang, J., Hu, A., Peng, M., Huang, K., Fan, D., et al. (2021). COVID-19 induces new-onset insulin resistance and lipid metabolic dysregulation via regulation of secreted metabolic factors. Signal Transduct. Target. Ther. *6*, 427.

86. Tyanova, S., Temu, T., and Cox, J. (2016). The MaxQuant computational platform for mass spectrometry-based shotgun proteomics. Nat. Protoc. *11*, 2301–2319.

Please cite this article in press as: Huang et al., Gut microbial co-metabolite 2-methylbutyrylcarnitine exacerbates thrombosis via binding to and activating integrin α2β1, Cell Metabolism (2024), https://doi.org/10.1016/j.cmet.2024.01.014

STAR★METHODS

KEY RESOURCES TABLE

REAGENT or RESOURCE	SOURCE	IDENTIFIER
Antibodies		
Rabbit polyclonal anti-cPLA2	Cell Signaling Technology	Cat#2832; RRID: AB_2164442
Rabbit polyclonal anti-p-cPLA2	Cell Signaling Technology	Cat#2831; RRID: AB_2164445
Rabbit monoclonal anti-p38	Cell Signaling Technology	Cat#8690; RRID: AB_10999090
Rabbit monoclonal anti-p-p38	Cell Signaling Technology	Cat#4511; RRID: AB_2139682
Rabbit monoclonal anti-Erk	Cell Signaling Technology	Cat#4695; RRID: AB_390779
Rabbit monoclonal anti-p-Erk	Cell Signaling Technology	Cat#4370; RRID: AB_2315112
Rabbit monoclonal anti-p-FAK	Immunoway	Cat#YP0515; RRID: AB_2936917
Rabbit polyclonal anti-FAK	Proteintech	Cat#12636-1-AP; RRID: AB_2173668
Rabbit polyclonal anti-PLCβ3	Immunoway	Cat#YT3790; RRID: AB_2936918
Rabbit polyclonal anti-p-PLCβ3	Immunoway	Cat#YP0707; RRID: AB_2936919
Rabbit polyclonal anti-c-Src	Immunoway	Cat#YT1136; RRID: AB_2927476
Rabbit polyclonal anti-p-c-Src	Immunoway	Cat#YP0078; RRID: AB_2936920
Rabbit monoclonal anti-integrin α2	Abcam	Cat#ab133557; RRID: AB_2833020
Rabbit monoclonal anti-integrin αIIb	Abcam	Cat#ab134131; RRID: AB_2732852
Rabbit monoclonal anti-GPIbα	Abcam	Cat#ab134087; RRID: AB_2936922
Rabbit polyclonal anti-P2Y1	Immunoway	Cat#YN2673; RRID: AB_2936921
Rabbit monoclonal anti-GAPDH	Cell Signaling Technology	Cat#5174; RRID: AB_10622025
Rabbit monoclonal anti-P-selectin	Invitrogen	Cat#MA1-81809; RRID: AB_2184952
Rabbilt monoclonal anti-SARS-CoV-2 Nucleocapsid Protein	GeneTex	Cat#GTX632269; RRID: AB_2888304
Anti-rabbit IgG, HRP-linked Antibody	Cell Signaling Technology	Cat#7074; RRID: AB_2099233
Bacterial and virus strains		
Wild-type SARS-CoV-2 virus strain	Guangzhou Customs District Technology Center	GenBank: MT123290
Biological samples		
Human stool	This paper	N/A
Human peripheral plasma	This paper	N/A
Chemicals, peptides, and recombinant proteins		
2-Methylbutyryl-L-carnitine (2MBC)	Sigma	Cat#50405
Isobutyryl-L-carnitine (IBC)	Sigma	Cat#51085
Hexanoyl-L-carnitine (HXC)	Sigma	Cat#91388
2-Methylbutyric acid (2MBA)	Sigma	Cat#193070
BTT 3033	TOCRIS	Cat#4724
MAFP	MedChemExpress	Cat#HY-103334
Aspirin	MedChemExpress	Cat#HY-14654
Heparin sodium	APExBIO	Cat#A5066
ADP	MedChemExpress	Cat#HY-W010918
Collagen	Chrono-Log	Cat#P/N385
Thrombin	Solarbio	Cat#T8021
Fibrinogen	Solarbio	Cat#F8051
Prostaglandin E1(PEG-1)	Sigma	Cat#P5515
Rhodamine 6G	Sigma	Cat#252433
Rose Bengal	Solarbio	Cat#G8540
$FeCl_3$	Aladdin	Cat#I141414

(*Continued on next page*)

Please cite this article in press as: Huang et al., Gut microbial co-metabolite 2-methylbutyrylcarnitine exacerbates thrombosis via binding to and activating integrin α2β1, Cell Metabolism (2024), https://doi.org/10.1016/j.cmet.2024.01.014

Continued

REAGENT or RESOURCE	SOURCE	IDENTIFIER
Evans Blue	Solarbio	Cat#E8010
Neomycin sulfate	MedChemExpress	Cat#HY-B0470
Streptomycin	MedChemExpress	Cat#HY-B1906
Bacitracin	MedChemExpress	Cat#HY-107193
Vancomycin	MedChemExpress	Cat#HY-B0671
Cefuroxime	MedChemExpress	Cat#HY-B1256
Piperacillin	MedChemExpress	Cat#HY-B1286
Levofloxacin	MedChemExpress	Cat#HY-B0330
Tyrode's salts solution	Coolaber	Cat#SL6510
Human integrin alpha2beta1 heterodimer protein	Acro Biosystems	Cat#IT1-H52W6
Recombinant integrin alpha2B	Cloud-Clone Corp.	Cat#RPB228Hu01
Critical commercial assays		
Rat Arachidonic Acid (AA) ELISA Kit	CUSABIO	Cat#CSB-E13008r
Rat D-dimer ELISA Kit	CUSABIO	Cat#CSB-E12984r
Rat Thromboxane B2 ELISA Kit	CUSABIO	Cat#CSB-E08047r
Mouse P-Selectin ELISA Kit	CUSABIO	Cat#CSB-E04709m
Mouse D-dimer ELISA Kit	CUSABIO	Cat#CSB-E13584m
Mouse Interleukin 6 ELISA Kit	CUSABIO	Cat#CSB-E04639m
Mouse Ferritin ELISA Kit	CUSABIO	Cat#CSB-E08827m
Thromboxane B2 Assay	R&D	Cat#KGE011
Cardiac troponin Assay Kit	Nanjing Jiancheng Bioengineering Institute	Cat#H149-2
Stool Genomic DNA Extraction Kit	Solarbio	Cat#D2700
Fatty Acid Oxidation Assay	Abcam	Cat#ab217602
Alanine aminotransferase Assay Kit	Nanjing Jiancheng Bioengineering Institute	Cat#C009-2-1
Aspartate aminotransferase Assay Kit	Nanjing Jiancheng Bioengineering Institute	Cat#C010-2-1
Creatinine Assay Kit	Nanjing Jiancheng Bioengineering Institute	Cat#C011-2-1
Thrombin colorimetry assay kit	GENMED SCIENTIFIC	Cat#GMS 50339.1.1
Deposited data		
I domain from integrin α2β1 structure	This paper	PDB: 1AOX
Metabolomics data	This paper; Dryad Digital Repository	https://doi.org/10.5061/dryad.m905qfv63
Phosphoproteomics data	This paper; Dryad Digital Repository	https://doi.org/10.5061/dryad.k6djh9wbq
Experimental models: Cell lines		
HEK-293T	ATCC	Cat#CRL-3216; RRID: CVCL_0063
Hela	ATCC	Cat#CRM-CCL-2; RRID: CVCL_0030
Experimental models: Organisms/strains		
Mouse: C57BL/6JGpt	Sun Yat-sen University	N/A
Mouse: B6/JGpt-Ace2em1Cin(hACE2)/Gpt	GemPharmatech	Cat#T037659; RRID: IMSR_GPT:T037659
C57BL/6JGpt-Itga2em17Cd16925/Gpt	GemPharmatech	Cat# T028416
Rat: Sprague Dawley	Zhuhai BesTest	N/A
Oligonucleotides		
GenOFF h-ITGA2	RIBOBIO	Cat#SIGS0001166-1
GenOFF h-ITGA2B	RIBOBIO	Cat#SIGS0001167-1
GenOFF h-GP1BA	RIBOBIO	Cat#SIGS0006506-1
GenOFF h-P2RY1	RIBOBIO	Cat#SIGS0000259-1
See Table S4 for the primers used in this study	N/A	N/A

(*Continued on next page*)

Please cite this article in press as: Huang et al., Gut microbial co-metabolite 2-methylbutyrylcarnitine exacerbates thrombosis via binding to and activating integrin α2β1, Cell Metabolism (2024), https://doi.org/10.1016/j.cmet.2024.01.014

Continued

REAGENT or RESOURCE	SOURCE	IDENTIFIER
Software and algorithms		
Graphpad Prism 9	GraphPad Software	Version 9.4.1
Image J	NIH	Version 1.51j8
Aggrolink8	Chrono-log	N/A
Analyst 1.6.3 software	Sciex	N/A
Agilent MassHunter Quantitative	Agilent	Version 10
Agilent MassHunter Qualitative	Agilent	Version 10
Vevo3100	VisualSonics	N/A
BIA evaluation	Cytiva	Version 4.1
R	https://www.r-project.org/	Version 4.1.2
Biorender	https://www.biorender.com/	N/A
VSTH	https://matgen.nscc-gz.cn/	N/A
Maestro	Schrödinger	Version 11.5
Other		
Chow diet	Xietong Shengwu	Cat#1010083
60% High fat diet	TROPHIC	Cat#TP23300

RESOURCE AVAILABILITY

Lead contact

Additional information and requests for resources and reagents should be addressed to the lead contact, Sifan Chen (chensf26@mail.sysu.edu.cn).

Materials availability

This study did not generate new unique materials or reagents.

Data and code availability

- All of the data supporting this study are included in the article.
- The metabolomics, phosphoproteomics, and 16S rDNA sequencing data have been deposited in the Dryad Digital Repository (https://doi.org/10.5061/dryad.m905qfv63; https://doi.org/10.5061/dryad.k6djh9wbq; https://doi.org/10.5061/dryad.x95x69prv).
- All raw data used to generate the figures throughout the manuscript can be found within the Data S1 document.
- This paper does not report original code.
- All additional datasets included in the manuscript will be provided upon request from the lead contact.

EXPERIMENTAL MODEL AND SUBJECT DETAILS

COVID-19 Subjects and Study Design

For cohort 1, to identify the altered metabolites upon SARS-CoV-2 infection, COVID-19 patients hospitalized in Guangzhou Eighth People's Hospital between January 22, 2020 and April 10, 2020 were enrolled. The diagnosis of COVID-19 was confirmed by two consecutive positive reverse transcriptase-polymerase chain reaction (RT-PCR) tests for SARS-CoV-2 infection. The disease severity was assessed according to the Chinese Government Diagnosis and Treatment Guideline for COVID-19 (Trial 7th version),[78] which classified the COVID-19 patients into four subgroups including mild, typical, severe and critical groups. In this study, mild and typical patients were composed into the non-Severe group, while severe and critical patients were composed into the Severe group. The exclusion criteria were: (1) probiotics, proton pump inhibitors or hormone drugs usage in the past one month; (2) with a history of autoimmune disease or chronic inflammatory bowel disease. In total, 64 COVID-19 individuals including 30 in the non-Severe group and 34 in the Severe group were recruited in this study. All of the non-Severe patients were without usage of antibiotics, whereas majority of the Severe patients received intravenous antibiotics therapy based on the disease severity. The clinical characteristics and laboratory parameters of these patients were described in Tables S1 and S2. We also procured 12 non-COVID-19 cases who had been exposed to COVID-19 patients, and presented with fever or cough. These 12 cases were hospitalized at the same period but determined as negative by two consecutive nucleic acid tests of SARS-CoV-2. For all patients, the inpatient diets were supplied by the hospital during hospitalization. Most of the fecal samples from non-severe or non-COVID-19 patients were collected within 3 days after hospital admission, except for samples from the Severe group were performed at later stages. Moreover, fecal samples from 12 healthy volunteers working at Guangzhou Eighth People's Hospital were collected as control (Figure 1A). For cohort 2, to

Please cite this article in press as: Huang et al., Gut microbial co-metabolite 2-methylbutyrylcarnitine exacerbates thrombosis via binding to and activating integrin α2β1, Cell Metabolism (2024), https://doi.org/10.1016/j.cmet.2024.01.014

investigate the alterations of gut metabolites during different periods of SARS-CoV-2 infection, 28 patients (including 12 non-severe and 16 severe ones) from cohort 1 were enrolled. All the patients received a 14-day medical quarantine in hospital after virus clearance (defined as at least two consecutive negative nucleic acid tests), and thereafter, attended outpatient follow-up during the first month after discharge. Fecal samples were collected in indicated time as shown in Figure 1A. All fecal samples were subjected to viral inactivation under 56 °C for at least 30 min and stored at -80 °C for further metabolomics analysis. The retrospective cohort study was approved by the Institutional Review Board of Guangzhou Eighth People's Hospital, with written informed consent collected.

Blood Collection

To measure the circulating levels of 2-methylbutyrylcarnitine, isobutyrylcarnitine and hexanoylcarnitine, plasma samples from COVID-19 subjects at acute-phase and healthy volunteers were obtained. The study was approved by the Institutional Review Board of Guangzhou Eighth People's Hospital. All patients provided written informed consent. Plasma samples were collected after fasting overnight and centrifuged with 3,000 × *g* 10 min at 4 °C. Subsequently, viral inactivation was conducted under 56 °C for 30 min and then the samples were store at -80 °C. In an additional study, plasma samples from subjects diagnosed with ACS, AIS, severe pneumonia, and healthy individuals were obtained from the First Affiliated Hospital of Sun Yat-sen University, with the approval by the Institutional Review Board. All patients and heathy volunteers provided written informed consent. Plasma samples were obtained from enrolled patients at admission and stored at -80 °C.

Animal Studies

Six-eight weeks old specific pathogen-free (SPF) C57BL/6J mice as well as Sprague-Dawley (SD) rats were purchased from Animal Center of the First Affiliated Hospital of Sun Yat-sen University or Zhuhai BesTest (Zhuhai, China), respectively. For *in vivo* integrin α2 knockout experiments, ten-week-old male α2-/- mice on C57BL/6J background (edited by CRISPR/Cas9 technology) were purchased from GemPharmatech (Jiangsu, China). All animals were housed under SPF conditions in a control environment (12-hour day/night cycle) under 23 ± 2 °C temperature and 50-60% humidity, with free access to food and water. All animals were fed a standard chow diet (Xietong Shengwu, China) unless otherwise indicated. For all studies, except for the pulmonary artery thrombosis assay, male mice and rats were used. All animal experiments were performed in accordance with the Guidelines for the Care and Use of Laboratory Animals and were approved by the Institutional Animal Care and Use Committees of the First Affiliated Hospital of Sun Yat-sen University.

For SARS-CoV-2-infected study, five-week-old male human ACE2 homogeneous knock in mice (with replacement of endogenous mouse ACE2) were purchased from GemPharmatech (Jiangsu, China), and the experiment was performed at the BSL-3 facilities with the approval of the Institutional Animal Care and Use Committees of Guangzhou Customs District Technology Center.

Cell Culture

HEK-293T cells (female) were cultured in Dulbecco's modified Eagle's medium (DMEM, Hyclone) supplemented with 10% FBS at 37 °C in a 5% CO_2 cell culture incubator. Lipofectamine RNAIMAX (Invitrogen, USA) was used for siRNA transfections according to the manufacturers' instructions. HEK-293T cells cultured in 12-well plate were transfected with siRNA in a final concentration of 100 nM for 48 h for the siRNA knockdown experiments. Afterwards, HEK-293T cells were treated with indicated concentration of vehicle or 2MBC, then harvesting for RNA or protein analysis.

Platelet Rich Plasma or Washed Platelet Isolation from Human Donors

Whole blood was collected from the authors (K.H., D.F., Z.Z., C.L) by peripheral venous punctured with 9:1 sodium citrate (0.38%). Platelet rich plasma (PRP) was separated by centrifuging at 200 × *g* for 10 min at 22 °C. Platelet poor plasma (PPP) was prepared by further centrifugation at 1,500 × *g* for 15 min. For the preparation of washed platelet, 100 nM prostaglandin E1 (PGE-1) was added to PRP and then centrifuged at 500 × *g* for 20 min at 22 °C. The platelet pellet was gently washed with a Ca^{2+} free modified Tyrode's buffer (Coolaber, China) with 100 nM PGE-1, and centrifuged again at 500 × *g* for 20 min. Platelet pellets were then re-suspended in modified Tyrode's buffer with 0.35% bovine serum albumin (BSA) and subjected to platelet aggregometry assay.

Platelet Rich Plasma or Washed Platelet Isolation from Rodent

For *ex vivo* platelet rich plasma preparation, 6-8 weeks old male C57BL/6J mice were anesthetized with 1% pentobarbital sodium (80 mg/kg). Whole blood (600 μL) was collected directly by cardiac punctured into 100 μL sodium citrate (0.38%) and then diluted with an additional 500 μL Ca^{2+} free modified Tyrode's buffer. Diluted platelet rich plasma was separated by centrifuging at 100 × *g* for 10 min at 22 °C. Diluted platelet poor plasma was prepared by further centrifugation at 1,500 × *g* for 15 min.

For *in vitro* studies, male SD rats (200-250 g) were anesthetized with 1% pentobarbital sodium (80 mg/kg). Whole blood was collected by cardiac punctured with 6:1 sodium citrate (0.38%) and then diluted with Ca^{2+} free modified Tyrode's buffer. Diluted platelet rich plasma was separated by centrifuging at 200 × *g* for 20 min at 22 °C. Diluted PPP was prepared by further centrifugation at 1,500 × g for 15 min. In some experiments, for preparation of washed platelet, 100 nM PGE-1 was added to PRP and then centrifuged at 500 × *g* for 20 min at 22 °C. The platelet pellet was gently washed with a Ca^{2+} free modified Tyrode's buffer with 100 nM PGE-1, and centrifuged again at 500 × *g* for 20 min. Platelet pellets were then re-suspended in modified Tyrode's buffer with 0.35% BSA and subjected to subsequent experiments.

Please cite this article in press as: Huang et al., Gut microbial co-metabolite 2-methylbutyrylcarnitine exacerbates thrombosis via binding to and activating integrin α2β1, Cell Metabolism (2024), https://doi.org/10.1016/j.cmet.2024.01.014

METHOD DETAILS

Untargeted Liquid Chromatography-Mass Spectrometry (LC-MS/MS) Analysis

Samples were thawed on ice. 50 mg of each sample was homogenized with 500 μL of ice-cold methanol/water (70%, v/v) with internal standard including L-2-chlorophenylalanine, L-carnitine-d3 HCl, 4-fluoro-L-α-phenylglycine, L-phenylalanine-2-13C, hippuric acid-d5, kynurenic acid-d5 and phenoxy-d5-acetic acid. The mixture was then centrifuged with 14,000 × *g* at 4 °C for 10 min. Thereafter, the supernatant was extracted and taken for LC-MS analysis. LC-MS analysis was conducted using an LC-ESI-MS/MS system (UPLC, ExionLC AD, https://sciex.com.cn/; MS, QTRAP System, https://sciex.com/). The analytical conditions were as follows, UPLC: column, Waters ACQUITY UPLC HSS T3 (1.8 μm, 2.1 mm × 100 mm); column temperature, 40 °C; flow rate, 0.4 ml/min; injection volume, 2 μL; solvent system, 0.1% formic acid in water: 0.1% formic acid in acetonitrile (ACN); gradient program, 95:5 V/V at 0 min, 10:90 V/V at 10.0 min, 10:90 V/V at 11.0 min, 95:5 V/V at 11.1 min, 95:5 V/V at 14.0 min. LIT and triple quadrupole (QQQ) scans were acquired on a triple quadrupole-linear ion trap mass spectrometer (QTRAP), QTRAP® LC-MS/MS System, equipped with an ESI Turbo Ion-Spray interface, operating in positive and negative ion mode and controlled by Analyst 1.6.3 software (Sciex). The ESI source operation parameters were as follows: source temperature 500 °C; ion spray voltage (IS) 5500 V (positive), -4500 V (negative); ion source gas I (GSI), gas II (GSII) and curtain gas (CUR) were set at 55, 60, and 25.0 psi, respectively; the collision gas (CAD) was high. Instrument tuning and mass calibration were performed with 10 and 100 μmol/L polypropylene glycol solutions in QQQ and LIT modes, respectively. A specific set of multiple reaction-monitoring (MRM) transitions were monitored for each period according to the metabolites eluted within this period.

Targeted LC-MS/MS Analysis

Samples were thawed on ice. 50 μL of each plasma sample was homogenized with 200 μL of ice-cold methanol containing internal standard ((±)-2-Methylbutyryl-L-carnitine-d3 chloride, d3-2MBC), followed by vortexing and centrifuging with 14,000 × *g* at 4 °C for 10 min. Subsequently, the supernatant was extracted and lyophilized by using a freeze dryer, and then the lyophilized powder was dissolved with 50 μL 50% acetonitrile. Then the clear supernatant was transferred to glass vials with microinserts and LC-MS/MS analysis was performed on Agilent 129II Infinity UHPLC -6470B Triple quadrupole LC-MS system (GENTECH SCIENTIFIC, USA). For chromatographic separation, a Thermo Hypersil Gold C18 column (2.1 × 100 mm, 1.9 μm) was used. The mobile phase consisted of solvent A (0.1% formic acid in water) and solvent B (0.1% formic acid in ACN) were run using the following gradient: 0-0.5 min, 5% B, 0.5-3 min, 5%→95%B, 3-3.5 min, 95%→5%B). Afterwards, 5%B was used to equilibrate the column for 5 min. The flow rate was 0.3 mL/min with a 1 μL injection volume. MRM in positive electrospray ionization mode (Agilent Jet Stream) was used with the following transitions: d3-2MBC at *m/z* 249.1 → 85.1 and *m/z* 249.1 → 187.0; 2MBC at *m/z* 246.1 → 85.1 and *m/z* 246.1 → 187.1. The following ion source parameters were as follows: gas temperature, 300 °C; gas flow, 5 L/min; nebulizer, 45 psi; sheath gas flow, 11 L/min; capillary, 3500 V (positive); 3500 V (negative); nozzle voltage charging, 500 V (positive), 500V (negative). 2MBC was quantified according to the standard curve running at the same batch of samples.

16S rDNA Sequencing

Fecal samples were profiled for bacterial taxa using 16S rDNA gene sequencing as previously reported.[79] Briefly, microbial DNA was extracted from feces samples using the FastDNA SPIN Kit (MP Biomedicals, USA) according to the manufacture's protocol. Amplification and sequencing of the V4 hypervariable region of the 16S rRNA gene was performed using the validated, region-specific bacterial primers 515F and 806R. The PCR conditions consisted of an initial denaturation step of 95°C for 3 min; 30 cycles of 98°C for 1 min, 98°C for 10 s, 50°C for 30 s, 72°C for 30 s, followed by 72°C for 5 min. Replicate amplicons were pooled and purified using with the AxyPrep DNA purification Kit (AXYGEN). Subsequently, paired-end sequencing was performed using the Miseq PE150 platform (Illumina, USA). Operational taxonomic units (OTUs) were picked at 97% sequence similarity using Greengene bacterial database for taxonomy information. Microbial composition at each taxonomic level was defined using the summarize_taxa function in Quantitative Insights Into Microbial Ecology (QIIME). The abundance of each taxon was calculated by dividing the sequences pertaining to a specific taxon by the total number of bacterial sequences for that sample.

Carotid Artery $FeCl_3$ Injury Thrombosis Assay

Six-to-eight weeks old male C57BL/6J mice were administrated with indicated doses of 2MBC for 2 h, then were anesthetized with 1% pentobarbital sodium (80 mg/kg) and subjected to a common carotid artery injury as previously described.[16] Briefly, Rhodamine 6G (100 μL; 0.5 μg/mL) was injected directly into the right jugular vein to label platelets. The left carotid artery was exposed and injured by placing 2 × 1.5 mm^2 Whatman filter paper soaked in 7.5% $FeCl_3$ solution to the surface of the vessel for 1 min. After removing the paper, the surface of the vessel was rinsed with saline. Thrombus formation was observed in real time using fluorescence stereomicroscope (Leica, Germany). Time to cessation of blood flow through clot formation for all studies was determined by visual inspection by two independent investigators. The end points were set as complete cessation of blood flow for more than 1 min or occlusion is not observed in 30 min after injury.

Photochemical Injury Thrombosis Assay

Eight weeks old male C57BL/6J mice were administrated with indicated doses of 2MBC for 2 h, then were anesthetized with 1% pentobarbital sodium (80 mg/kg). Rose Bengal (20 mg/mL in saline) was injected directly into tail vein to a dose of

100 mg/kg. Rhodamine 6G (100 μL; 0.5 μg/mL) was injected directly into the right jugular vein to label platelets. The left carotid artery was isolated and illuminated with green light laser source and real-time monitored by MICRON IV Retinal Imaging microscope (Phoenix, Germany). The time to occlusion was determined after the vessel remained closed for 3 minutes.

Thrombin Induced Pulmonary Artery Thrombosis Assay

Thrombin induced pulmonary artery thrombosis assay was performed as described with slight modifications.[31] Eight weeks old female C57BL/6J mice were administrated with indicated doses of 2MBC for 2 h, then were anesthetized with 1% pentobarbital sodium (80 mg/kg) and thrombin (200 U/kg) was slowly injected into the right jugular vein. Animals surviving from the challenge for more than 30 min were considered survivors. Once the respiratory arrest onset or animals survive for more than 30 min, 0.5 mL Evans blue solution (1% in saline) was infused via the inferior vena cava while the heart still beating. Afterwards, lungs were excised and were rinsed by distill water for 1 min to remove the Evans blue dye that retained in the interstitial space, then photographed. Lung infarction score was recorded according to the area of Evans blue staining. Zero indicates no leakage (entirely pink) and four indicates complete leakage (entirely blue). In some experiments, a lower non-lethal dose of thrombin (40 U/kg) was injected to maintain the animals survive. Echocardiography was performed 2 h later to investigate the pulmonary arterial pressure.

Echocardiography

Echocardiography was performed using Vevo3100 (VisualSonics, Canada) equipped with a 30 MHz linear transducer (Visual Sonics, Canada) as previously described.[80] Two-dimensional images of the pulmonary infundibulum were obtained from the parasternal short axis view at the level of the aortic valve and pulsed-wave Doppler recording of the pulmonary blood flow was obtained. The Pulsed-wave Doppler sample was positioned at the tip of the pulmonary valve leaflets and aligned to maximize laminar flow. Doppler tracings were recorded at a sweep speed of 400 mm/sec. Measurements were performed offline (Vevo 770 workstation) by two independent investigators. The following variables were measured: mean pulmonary artery pressure (mPAP), peak velocity (Peak Vel) and pulmonary acceleration time (PAT, defined as the time from the onset of flow to peak velocity by pulsed-wave Doppler recording). All measurements were averaged on 3 cardiac cycles.

In Vivo 2MBA Challenge Study

Six weeks old male C57BL/6J mice were fasted for 4 h and then administered with 2MBA (50 μg/kg) via oral gavage or intraperitoneal injection. Plasma was dynamically collected from the angular vein at 0, 30, 60 and 120 min for 2MBC quantification by targeted mass spectrometry analysis. In some experiments, mice were pre-treated with vancomycin (0.5 mg/mL), cefuroxime (1 mg/mL), piperacillin (1 mg/mL), levofloxacin (0.1 mg/mL) or combination of cefuroxime (1 mg/mL) and levofloxacin (0.1 mg/mL), respectively, in drinking water for five consecutive days. Then, plasma samples were collected at the indicated time points following 2MBA (50 μg/kg) oral gavage for 2MBC detection.

In Vivo Fasting/Re-feeding Study

Six weeks old male C57BL/6J mice were treated with an antibiotic cocktail in drinking water to eliminate gut microbiota as previously described.[81] Briefly, mice were given an antibiotic cocktail in the drinking water consisting of neomycin (1 mg/mL), streptomycin (1 mg/mL) and bacitracin (1 mg/mL) for 5 days. Afterwards, all mice were food-deprived for 18 h. Fasted mice were then given access to chow diet for 6 h at the beginning of the light cycle and plasma samples were collected immediately following this re-feeding period for 2MBC quantification.

Murine Antibiotic Challenge and Fecal Microbial Transplantation Study

Eight-week-old male C57BL/6J mice were treated with an antibiotic cocktail as mentioned above. For microbial recolonization, after treatment of antibiotic cocktail, mice were co-housing with conventionally reared littermates by 1:1 ratio in a single cage for another 7 days. Fecal samples were collected at the end of the experiments and bacterial DNA was extracted using Stool Genomic DNA Extraction Kit (Solarbio Life Sciences, China) according to the manufacturer's instruction. Thereafter, Realtime qPCR targeting 16S ribosomal DNA was conducted to determine the bacterial load of stool.

In Vivo SARS-CoV-2-infected Study

Five weeks old male human ACE2 transgenic mice were fed with 60% high fat diet (HFD; TP23300, TROPHIC, China) for 18 weeks and were intranasally inoculated with 5,000 50% tissue culture infectious dose ($TCID_{50}$) per mouse of wild-type SARS-CoV-2 virus strain (GenBank accession No. MT123290), then followed by daily intraperitoneal injection of BTT 3033. hACE2 mice that intranasally inoculated with vehicle were set as the control. Body weight was recorded daily. For the antibiotics challenge group, mice were pre-treated with antibiotic cocktail as mentioned above for 3 days before SARS-CoV-2 inoculation and maintained until the end of the study. After 7 days of infection, all mice were fasted for 6 h and then euthanized for samples collection.

In Vitro Fecal Fermentation Assay

Fresh colonic fecal samples from C57BL/6J mice fed with chow diet were collected and proceeded within 30 min. The 20% (w/v) fecal slurry was prepared by diluting the homogenized fecal sample in sterile phosphate buffered saline (PBS) medium. After a centrifugation of 500 × *g* at room temperature for 10 min, the supernatant was collected and cultured with thioglycolate medium in an

Please cite this article in press as: Huang et al., Gut microbial co-metabolite 2-methylbutyrylcarnitine exacerbates thrombosis via binding to and activating integrin α2β1, Cell Metabolism (2024), https://doi.org/10.1016/j.cmet.2024.01.014

anaerobic chamber at 37 °C overnight without stirring. Optical density at 600 nm (OD600) of the bacterial culture was determined and adjusted to 2.0. Then, 1 mL of bacterial culture was centrifugated with 1500 × *g* at room temperature for 10 min and re-suspended by equal volume of sterile PBS with 2MBA (200 μM) or its vehicle. Afterwards, it was further incubated in an anaerobic chamber at 37 °C without stirring. Samples were dynamically collected at indicated time point for 2MBC quantification.

Histological and Immunohistochemical Studies

All tissues were fixed in 4% paraformaldehyde for 24 h, embedded in paraffin and sectioned (5 μm). All tissue sections were stained with Hematoxylin and Eosin (H&E) by standard staining procedure. Immunohistochemistry was conducted as previously described[79] using antibody against CD62P (Invitrogen, USA, 1:100 dilution), SARS-CoV Nucleoprotein (GeneTex, China, 1:100 dilution), then stained sections were digitally captured. For the quantitative analysis of CD62P expression in thrombi within the carotid artery, the percentage of the stained area (the stained area per total lumen area) was calculated and quantified by histomorphometry using ImageJ software (National Institutes of Health, USA). For the quantitative analysis of thrombi, CD62P expression or SARS-CoV Nucleoprotein (integrated optical density) and lung injury score (histological findings of neutrophils in the alveolar space, neutrophils in the interstitial space, hyaline membranes, proteinaceous debris filling the airspaces and alveolar septal thickening),[82] 5 random fields were captured from different areas of a single section, and then analyzed by ImageJ software.

Platelet Aggregometry Assay

Platelet aggregometry assays were performed as previously described.[16] Typically, platelets were counted using an automated hemocytometer (Mindray, China) and concentrations adjusted to 2 × 10^8/mL with platelet poor plasma or modified Tyrode's buffer. Platelets were then pre-incubated with 2MBC (0.5 μM or at indicated concentrations) for 30 min. Afterwards, indicated concentration of $CaCl_2$ and/or $MgCl_2$ were added immediately before platelet aggregation studies. Platelet aggregation was assessed at 37 °C in a dual channel Type 700 aggregometer (Chrono-log Corporation, US) with stirring at 1,000 rpm.

Platelet Spreading Assay

Glass coverslips were pre-coated with collagen (20 μg/mL) at 4 °C overnight. Rat platelets pre-incubated with or without 2MBC (0.5 μM) were allowed to spread on the collagen-coated surfaces at 37 °C for 60 min followed by fixation, permeabilization and staining with Rhodamine 6G. Adherent platelets were detected under a fluorescence microscopy (DMI8, Leica, Germany). The surface coverage was quantified using Image J software (National Institutes of Health, USA).

Clot Retraction Assay

Clot retraction was performed as described previously.[83] Briefly, 2 mM Ca^{2+} and 0.5 mg/ml fibrinogen were added to the PRP at a platelet concentration of 2 × 10^8/mL. Clot retraction was initiated by the addition of 1 U/mL thrombin and allowed proceed at 37 °C. Images were captured at 0, 15, 30 and 60 min, respectively.

Coagulant Assay

The activated partial thromboplastin time (APTT) was performed by mixing 50 μL thawed citrated plasma with 50 μl pre-warmed APTT reagent (Helena Laboratories) in a glass tube and incubated for 5 min at 37 °C. The reaction was initiated by adding 50 μL 35.3 mM $CaCl_2$. The endpoint clotting time was determined visually by constantly tilting the cuvette in a 37 °C water bath. The prothrombin time (PT) was performed similarly by the addition of 100 μL of pre-warmed PT reagent (Thromboplastin Reagent, Helena) to 50 μL thawed citrated in a glass tube.

Thrombin Activity Assay

Six-week-old male C57BL/6J mice were *i.p.* injected with saline or 2MBC (100 μg/kg) for 2 h. Afterwards, plasma samples were collected for *ex vivo* thrombin activity assay using a commercial assay kit (GENMED Scientifics, USA) according to the manufacturer's protocol.

Tail Bleeding Assay

Tail bleeding assay was performed as described previously.[84] Mice were anesthetized with 1% pentobarbital sodium (80 mg/kg). The tip of the tail (2 mm) was cut and the injury tail was immediately placed into pre-warmed PBS at 37 °C for 10 min. The hemoglobin content was determined by measuring the absorbance at 550 nm using a microplate reader (Tecan, Astria).

Biochemical Index Analysis

Six-week-old male C57BL/6J mice were *i.p.* injected with BTT 3033 (1 mg/kg) or its vehicle for 3 days, then subjected to $FeCl_3$-induced carotid artery injury thrombosis assay. Afterwards, plasma samples were collected for the analysis of alanine aminotransferase, aspartate aminotransferase, and creatinine using commercial assay kits (Nanjing Jiancheng Bioengineering Institute, China) according to the manufacturer's protocol.

Please cite this article in press as: Huang et al., Gut microbial co-metabolite 2-methylbutyrylcarnitine exacerbates thrombosis via binding to and activating integrin α2β1, Cell Metabolism (2024), https://doi.org/10.1016/j.cmet.2024.01.014

Immunoblot Studies

For Western blotting, cells and tissues were lysed in RIPA buffer (Tris-HCl 25 mM, pH 7.6; NaCl 150 mM; NP-40 1%; sodium deoxycholate 1%; SDS 0.1%) with protease inhibitors and phosphatase inhibitors. Protein concentration was measured using bicinchoninic acid (BCA) (ComWin Biotech, China). Equal amounts of protein were separated by SDS-PAGE and transferred to a polyvinylidene difluoride (PVDF) membrane which was incubated in 5% milk in Tris-buffered saline for 1 h at room temperature, followed by incubation with primary antibodies against cPLA2 (Cell Signaling Technology, USA, 1:1,000 dilution), p-cPLA2 (Cell Signaling Technology, USA, 1:1,000 dilution), p38 (Cell Signaling Technology, USA, 1:1,000 dilution), p-p38 (Cell Signaling Technology, USA, 1:1,000 dilution), Erk (Cell Signaling Technology, USA, 1:1,000 dilution), p-Erk (Cell Signaling Technology, USA, 1:1,000 dilution), PLCβ3 (Immunoway, USA, 1:1,000 dilution), p-PLCβ3 (Immunoway, USA, 1:1,000 dilution), Src (Immunoway, USA, 1:1,000 dilution), p-Src (Immunoway, USA, 1:1,000 dilution), FAK (Proteintech, China, 1:1,000 dilution), p-FAK (Abcam, UK, 1:1,000 dilution), integrin α2 (Abcam, UK, 1:1,000 dilution), integrin αIIb (Abcam, UK, 1:1,000 dilution), GPIb (Abcam, USA, 1:1,000 dilution), P2Y1 (Immunoway, USA, 1:1,000 dilution) and GAPDH (Cell Signaling Technology, USA, 1:1,000 dilution) overnight at 4 °C, and a secondary antibody (1:10,000 dilution) conjugated with horseradish peroxidase (Cell Signaling Technology, USA) for 1 h at room temperature. Membranes were developed with chemiluminescent ECL reagents (Millipore, USA). The relative expression of target protein to the control GAPDH or phosphorylated protein to the total protein were determined by densitometric analysis using ImageJ software (National Institutes of Health, USA).

RT-qPCR

RT-qPCR was conducted as previously described.[85] Briefly, total RNA was extracted by using AG RNAex Pro Reagent (Accurate Biotechnology, China). With 1 μg of total RNA for reverse transcription, cDNA was synthesized using Evo M-MLVRT Kit (Accurate Biotechnology, China). Real-time quantitative PCR was conducted with SYBR Green Permix Pro Taq HS qPCR Kit (Accurate Biotechnology, China) and LightCycle480 II thermal cycler (Roche, Switzerland). Relative expression of each gene was normalized to GAPDH. The value of the Ctrl group was set to 1. The sequences were listed in Table S4.

Enzyme-link Immunosorbent Assay (ELISA)

For the quantitative determination of plasma D-dimer, interleukin-6, ferritin, sCD62P, TXB2 and cardiac troponin concentrations in mice, plasma samples were diluted and added to ELISA assay plates pre-coated with specific antibodies. Samples were bound by the immobilized antibodies, reacted with avidin-conjugated Horseradish Peroxidase (HRP), and developed with 3,3',5,5'-tetramethylbenzidine (TMB) substrate. Reactions were terminated, and the absorbance was measured at 450 nm using a microplate reader (Tecan, Astria) within 5 min. In order to determine the changes of arachidonic acid (AA) and TXB2 under 2MBC treatment, rat PRP at a concentration of 2×10^8/mL was pre-incubated with 2MBC (0.5 μM) and/or MAFP (5 μM) for 30 min. Afterwards, platelet aggregation was initiated by ADP (5 μM) using a dual channel Type 700 aggregometer with constant stirring at 1,000 rpm. PRP samples were immediately frozen by liquid nitrogen to stop the reaction. Thereafter, samples were centrifuged with 14,000 × *g* at 4 °C for 10 min and the supernatant of each sample was collected for the measurements of AA (CUSHIBIO Biotech, China) or TXB2 (R&D, USA) respectively using an ELISA kit according to the manufacturer's instructions.

Fatty Acid Oxidation Assay

Washed platelets were seeded in the 96 well plates (black wall with clear flat bottom, Labselect, China) at a concentration of 1×10^7 platelets/well in 200 μL base measurement media (Abcam, UK) and 2.5 mM glucose according to manufacturer's instructions. For HEK-293T cells (female) and Hela cells (female), the cells were seeded in the 96 well plates at a concentration of 1×10^5 cells/well in 200 μL culture media and allowed to adhere to the plate for 24 h, followed by treated with glucose deprivation media for another 14 h. Subsequently, cells were incubated with indicated concentrations of 2MBC or oleate plus L-carnitine (positive control). The oxygen consumption rate was measured using a Victor Nivo 5S multimode microplate reader (PerkinElmer, USA) with the mode of time-resolved fluorescence (excitation filter 350/40 nm, emission filter 665/8 nm, delay time 30 μs, and emission time 100 μs) as recommended by the manufacturer.

Label-free Phosphorproteomics Analysis

For phosphorproteomics study, 2×10^8/mL of washed rat platelets were pre-incubated with or without 2MBC (0.5 μM) for 30 min. Afterwards, platelet aggregation was initiated by 1 U/mL thrombin using a dual channel Type 700 aggregometer with constant stirring at 1,000 rpm for 3 min. Thereafter, platelets were frozen by liquid nitrogen immediately to terminate the reaction, and then stored at -80 °C. Platelet samples were resuspended in an equal volume of lysis buffer (1.5% SDS/100 mM Tris-HCl, pH 8.5) and disrupted with ultrasound. Afterwards, proteins were extracted by acetone precipitation and dissolved in buffered solution (8 M Urea/100mM Tris-HCl, pH 8.5), then subjected to quantification by using bicinchoninic acid assay. Approximately 1 mg of protein per sample was alkylated with tris(2-carboxyethyl)phosphine and chloroacetamide at 37 °C for 1 h. 100 mM Tris-HCl was added to reduce the urea concentration to less than 2 M, then trypsin was added at a 50:1 protein:trypsin ratio. The samples were incubated overnight at 37 °C before quenching with trifluoroacetic acid (TFA). Phosphopeptides were enriched by incubating with TiO2 beads at 25 °C for 20 min, then the samples were eluted from the beads with TFA/ACN. Peptide samples were injected onto an Ionopticks Aurora Series UHPLC C18 column (75 μm × 250 mm, 1.6 μm particle size, 100 Å pore size). Solvent A (0.1% formic acid in water) and B (0.1% formic acid in ACN) were run using the following gradient: 0 min in 2% B; 50 min of 5-23% B; 10 min of 23-30% B); 5 min of 35-90% B; 10 min

of 90% B; with a flow rate of 0.3 μl/min. The timsTOF Pro system (Bruker Daltonics, Germany) was operated in positive mode with enabled trapped ion mobility spectrometry (TIMS) at 100% duty cycle (100 ms ramp time). Scan mode was set to parallel accumulation–serial fragmentation (PASEF). RAW instrument files for the phosphopeptide enrichment experiments were processed using MaxQuant software (version 3.03).[86]

Surface Plasmon Resonance (SPR) Assay

The SPR assays were performed to analyze the interactions between the compounds and proteins by using a Biacore T100 machine with Sensor Chip CM7 (GE Healthcare, USA) at 25 °C. Purified integrin α2β1 or integrin αIIbβ3 protein was immobilized onto CM7 chips, sensorgrams were recorded by injecting various concentrations of compounds. The binding kinetics (Kd) values of compounds binding to proteins were calculated based on the fitted curves using BIA evaluation Version 4.1 software.

QUANTIFICATION AND STATISTICAL ANALYSIS

Analyses were performed using Prism 9 (GraphPad Software, La Jolla, CA) unless otherwise indicated. Data were shown as the means ± SEM. All results shown were representative of at least three biological independent experiments. Normal distribution of data was assessed with the Shapiro-Wilk test. Unpaired Student's t-test or Welch's t-test was used for comparing differences between groups, depending on the distribution of these data. In multiple-group analysis, one-way ANOVA with Fisher's LSD post hoc test or Brown-Forsythe and Welch ANOVA followed by unpaired *t* with Welch's correction were used depending on the distribution of these data. Two-way ANOVA with Bonferroni's multiple comparisons test was used for comparing differences between groups with two or more independent variables. Kaplan-Meier analysis was used for time-to-event analysis to determine the survival rate of pulmonary artery thrombosis mice model, *P value*s was calculated by Log-rank (Mantel-Cox) test. Correlation analysis was shown as linear regression. Correlation coefficient *r* and significance of differences were calculated by using the nonparametric spearman's correlation test. All reported *P value*s were two-sided. For all tests, $p < 0.05$ was considered significant. All data points in the manuscript represented individual biological replicates unless otherwise indicated.